QUANTITATIVE BACKSCATTERED ELECTRON ANALYSIS TECHNIQUES FOR CEMENT-BASED MATERIALS

By

Hong Zhao
David Darwin

A Report on Research Sponsored by
THE AIR FORCE OFFICE OF SCIENTIFIC RESEARCH
Research Grant AFOSR-89-0296

The University of Kansas
Lawrence, Kansas
June 1990

SECURITY CLASSIFICATION OF THIS PAGE

REPORT DOCUMENTATION PAGE

1a. REPORT SECURITY CLASSIFICATION Unclassified	1b RESTRICTIVE MARKINGS
2a. SECURITY CLASSIFICATION AUTHORITY	3. DISTRIBUTION/AVAILABILITY OF REPORT Approved for public release; distribution is unlimited.
2b. DECLASSIFICATION/DOWNGRADING SCHEDULE	
4. PERFORMING ORGANIZATION REPORT NUMBER(S)	5. MONITORING ORGANIZATION REPORT NUMBER(S)
6a. NAME OF PERFORMING ORGANIZATION University of Kansas Center for Research, Inc. 6b. OFFICE SYMBOL (If applicable)	7a. NAME OF MONITORING ORGANIZATION Air Force Office of Scientific Research
6c. ADDRESS (City, State, and ZIP Code) Lawrence, KS 66045	7b. ADDRESS (City, State, and ZIP Code) AFOSR/NA Bolling Air Force Base Washington, DC 20332
8a. NAME OF FUNDING/SPONSORING ORGANIZATION 8b. OFFICE SYMBOL (If applicable)	9. PROCUREMENT INSTRUMENT IDENTIFICATION NUMBER AFOSR-89-0296
8c. ADDRESS (City, State, and ZIP Code)	10. SOURCE OF FUNDING NUMBERS PROGRAM ELEMENT NO. / PROJECT NO. / TASK NO. / WORK UNIT ACCESSION NO.

11. TITLE (Include Security Classification)

Quantitative Backscattered Electron Analysis Techniques for Cement-Based Materials

12. PERSONAL AUTHOR(S)
Zhao, Hong, and Darwin,David

13a. TYPE OF REPORT	13b. TIME COVERED FROM 890401 TO 900604	14. DATE OF REPORT (Year, Month, Day)	15. PAGE COUNT
		900604	59

16. SUPPLEMENTARY NOTATION

17. COSATI CODES			18. SUBJECT TERMS (Continue on reverse if necessary and identify by block number)
FIELD	GROUP	SUB-GROUP	backscattered electron imaging, backscattering coefficient, calibration, cement paste, cracking, epoxy impregnation, gray levels, hydration, image analysis,

19. ABSTRACT (Continue on reverse if necessary and identify by block number)

Backscattered electron imaging and x-ray microanalysis are used to identify phases within polished epoxy impregnated cement paste sections. A silicon-magnesium standard is applied and an objective procedure is developed for the calibration of the scanning electron microscope and the image analysis system, so that the intensity of individual phases in cement paste appears within reproducible ranges when using backscattered electron imaging. The techniques allow for consistency in quantitative analysis of cement microstructure. Image analysis of cement phases is carried out and a statistical basis is established for the number of frames that must be analyzed to obtain a satisfactory level of confidence in the data.

Backscattered electron imaging of polished surfaces of cement paste can be used to distinguish the phases within unhydrated cement particles and the phases of cement hydration products. The existence of calcium hydroxide within inner product is confirmed. For image analysis, the number of frames required for a selected level of con-

20. DISTRIBUTION/AVAILABILITY OF ABSTRACT ☐ UNCLASSIFIED/UNLIMITED ☐ SAME AS RPT. ☐ DTIC USERS	21. ABSTRACT SECURITY CLASSIFICATION unclassified
22a. NAME OF RESPONSIBLE INDIVIDUAL Dr. Spencer T. Wu	22b. TELEPHONE (Include Area Code) (202) 767-6962 22c. OFFICE SYMBOL AFOSR/NA

DD FORM 1473, 84 MAR 83 APR edition may be used until exhausted. All other editions are obsolete

SECURITY CLASSIFICATION OF THIS PAGE

18. (continued) intensities, microstructures, phases, polishing, quantitative analysis, standard, voids, x-ray dot mapping, x-ray microanalysis.

19. (continued) fidence decreases as the magnification decreases, while the total area required increases as the magnification decreases. To achieve a desired level of confidence in image analysis for the phases of hydrated cement paste, unhydrated cement particles require the greatest number of frames, while inner product and calcium silicate hydrate require the least number of frames.

INTRODUCTION

The scanning electron microscope (SEM) is a powerful tool for the study of cement-based materials. In recent years, this technique has been employed to investigate both fractured and polished surfaces of cementitious materials (Williamson 1972, Diamond 1976, Dalgleish and Pratt 1982, Attiogbe and Darwin 1985), allowing individual phases within hydrated cement to be identified (Williamson 1972, Diamond 1976, Scrivener and Pratt 1984, Scrivener et al. 1985, Scrivener and Gartner 1988). Different techniques for sample preparation have been developed during these investigations.

In the early work, interest was focused mainly on fractured surfaces in dried specimens (Williamson 1972, Diamond 1976, Dalgleish and Pratt 1982, Attiogbe and Darwin 1987) using secondary electron (SE) imaging. Sawed and polished surfaces were not used because polishing tended to damage the microstructure. To correct this problem, the technique of epoxy impregnation was developed (Scrivener and Pratt 1984, Struble and Byrd 1986, Struble and Stutzman 1988). Epoxy impregnation prevents damage during polishing because it effectively penetrates into the cement and, after hardening, supports the cement microstructure.

With the development of epoxy impregnation techniques, polished specimens were most often investigated using backscattered electron (BSE) imaging (Scrivener and Pratt 1984). The change from SE to BSE imaging was necessitated because secondary electrons provide only topographical data, which is not available from a smooth surface. In contrast, backscattered electrons carry little topographical information but, instead, provide atomic number contrast. The denser a material, the higher the intensity of its BSE signal. Therefore, specific phases within cement, such as unhydrated cement particles, calcium

hydroxide, inner product (the hydration product within the original boundary of the cement grain), calcium silicate hydrate, voids and cracks, can be identified based on the relative intensity of their BSE signals. Differences between the constituents of unhydrated cement particles can also be determined.

SE images do provide some atomic number contrast because secondary electron detectors (SED) pick up a small percentage of the backscattered electrons. The small BSE content in SE images, in fact, provides a useful purpose by helping create the "light optical analogy" that makes SE images so understandable. The reader is directed to Goldstein et al. (1981) or other basic SEM text for more information on SE imaging.

Scrivener and co-workers have used a backscattered electron detector (BSD) to differentiate phases within hydrated cement paste for several years (Scrivener and Pratt 1984, Scrivener et al. 1985, Scrivener and Gartner 1988, Scrivener 1989). In an early paper (Scrivener and Pratt 1984), the mean atomic numbers of the individual phases were calculated incorrectly, weakening some of the justification presented for using the technique. Scrivener later used image analysis to study the BSE intensities of individual phases within hydrated cement paste (Scrivener 1989). At that time, she reported that the unhydrated materials and calcium hydroxide had fairly uniform gray levels. However, this generalization is questionable, as will be discussed later in this report.

X-ray microanalysis also can be used to study cementitious materials. A number of investigators have applied the energy dispersive spectrometer (EDS) and/or the wavelength dispersive spectrometer (WDS) to the study the chemical composition of cement paste (Barnes, Jeffery and Sarkar 1978, Dalgleish and Pratt 1982). X-ray dot maps have been used to study polished clinker materials and identify constituents within clinker (Williamson 1972, Barker and Barnes 1984).

The studies discussed above demonstrate that the constituent phases within cement paste can be identified using the SEM and x-ray microanalysis. If quantitative information is desired, however, present BSE imaging techniques have major shortcomings. Without a way to establish standard settings, the apparent intensities of individual phases change each time an SEM and an image analysis system (IAS) are set up. These differences can be adjusted for by the operator; however, the adjustments are subjective. Procedures can be improved if a standard is developed so that the SEM and IAS can be adjusted objectively, insuring that each phase within cement paste will have a consistent intensity every time.

The purposes of this study are to 1) develop techniques for adjusting scanning electron microscope and image analysis systems, so that the intensity of individual phases in cement-based materials appear within reproducible ranges when using BSE imaging, and 2) establish a statistical basis for the number of frames that must be analyzed to obtain a satisfactory level of confidence in the data. The techniques will allow for consistency in quantitative analyses of cement microstructure.

BACKGROUND

The electron optical system in an SEM consists of an electron gun that emits electrons; condenser lenses and an objective lens that control the final beam current and focus the beam on the specimen; and electron and x-ray detectors that measure the signals. The distance between the objective lens and the specimen is known as the free working distance (FWD). Signals from beam electron-specimen interactions provide information about the specimen being studied.

Electron-specimen interactions can be generally described as elastic events, which

modify the trajectory of beam electrons, or inelastic events, which change the energy of the electrons. Elastic events produce backscattered electrons, while inelastic events produce secondary electrons, auger electrons, characteristic x-rays, and continuum x-rays. When elastic scattering occurs, the kinetic energy of the beam electrons, typically 10 keV or more, is little changed.

An understanding of the interaction between the beam electrons and the specimen is fundamental for the application of scanning electron microscopy to the study of cement. Beam electrons interact with the specimen over a region known as the interaction volume. Elastic and inelastic scattering are concurrent processes. Inelastic scattering progressively reduces the energy of a beam electron until it is captured by the specimen, thus limiting the range of travel of electrons within the solid. Since the travel of electrons is limited, it is expected that the signals detected will be from a certain region within the specimen. The sampling volume is the region from which emerging electrons and x-ray photons carry information about the nature of the specimen. Signals from different scattering processes carry information from different depths within the specimen. A schematic illustration of the interaction and sampling volumes is shown in Fig. 1.

The interaction volume is a function of the kinetic energy voltage of the incident electrons, as well as the target materials. One expression, derived by Kanaya and Okayama (1972), is widely used to calculate the size of interaction volume. Known as the K-O range,

$$R_{KO} = \frac{0.0276AE_0^{1.67}}{Z^{0.889}\rho} \quad \mu m \qquad (1)$$

in which A is the atomic weight, Z is the atomic number, E_0 is the energy of the beam

electrons and ρ is the density of the material.

The sampling volume for specific signals will be discussed individually.

Backscattered Electrons

Backscattered electrons are the result of elastic scattering. When beam electrons impinge on a target, some of the electrons penetrate into the target, expending all of their energy within the interaction volume. These electrons are absorbed by target materials. There is, however, a significant fraction of the beam electrons, which strike the target and are then scattered back out of the specimen. These reemergent electrons are known as backscattered electrons. The sampling volume for backscattered electrons is illustrated for silicon in Fig. 1. The sampling volume or sampling depth for BSE is approximately 30% of the K-O range. Electrons below the sampling depth are highly likely to be captured by the target material.

The tendency of electrons to backscatter is described by the backscattered electron coefficient, η, which is defined as

$$\eta = \frac{n_{bs}}{n_b} \qquad (2)$$

in which n_b is the number of beam electrons incident on the target and n_{bs} is the number of backscattered electrons.

The backscattering coefficient, η, is a function of atomic number, Z. For a pure element, η may be calculated as follows (Heinrich 1966).

$$\eta = -0.0254 + 0.016Z - 1.86\times10^{-4}Z^2 + 8.3\times10^{-7}Z^3 \qquad (3)$$

For a homogeneous mixture, the backscattering coefficient, η_{mix}, is calculated based on weight fractions of the elemental components (Heinrich 1966):

$$\eta_{mix} = \sum_i C_i \eta_i \qquad (4)$$

in which C_i is the weight fraction for element i and η_i is the backscattering coefficient of that element.

The mean atomic number $\bar{Z}$ of a mixture is calculated by

$$\bar{Z} = \sum_i C_i Z_i \qquad (5)$$

in which C_i and Z_i are the weight fraction and the atomic number, respectively, of element i.

Table 1 contains a list of the major elements in portland cement, along with their atomic numbers, atomic weights, and backscattering coefficients. For example, silicon (Si) has an atomic number of 14, atomic weight of 28.08, and a backscattering coefficient of 0.1644. Calcium (Ca), which has a higher atomic number and weight 20 and 40.08, has a higher backscattering coefficient 0.2268.

Table 2 presents the mean atomic numbers, $\bar{Z}$, and backscattering coefficients, η_{mix}, for the four major constituents in portland cement clinker, which are: tricalcium silicate (C_3S), dicalcium silicate (C_2S), tricalcium aluminate (C_3A) and tetracalcium aluminoferrite (C_4AF), and the major hydration products of portland cement, calcium hydroxide (CH), calcium silicate hydrate ($CSH_{1.5}$, $C_{1.5}SH_2$), ettringite ($C_3A\bar{S}_3H_{32}$) and calcium aluminate monosulphate ($C_3A\bar{S}H_{12}$) (Note: cement chemist's notation is used here and in Table 2).

The values of mean atomic numbers range form 16.65 for C_4AF to 10.76 for ettringite. The backscattering coefficients range from 0.1860 to 0.1233, for the same materials. Some discussion is necessary at this point.

There are five major phases that can be identified within hydrated cement paste using BSE imaging: 1) unhydrated cement particles, UH, 2) calcium hydroxide, CH, 3) inner product, IP, (which generally includes the hydration products within the original boundary of the cement grain, but here more specifically refers to hydration products other than calcium hydroxide, as will be explained later), 4) calcium silicate hydrate, CSH, and 5) voids and cracks. Based on the values shown in Table 2, it is obvious that the components of unhydrated particles have higher mean atomic numbers and backscattering coefficients than do the hydration products. Therefore, it is expected that unhydrated particles will have a higher BSE intensity than will the hydration products. Of the components of unhydrated cement, C_4AF has the highest mean atomic number and backscattering coefficient and, thus, C_4AF will have the highest intensity in a BSE image. Calcium hydroxide, has a relatively high mean atomic number and should appear brighter than the calcium silicate hydrates, and the other hydration products. An example of a BSE image of cement paste is shown in Fig. 2a. As predicted, the phases can be identified by their differences in intensity (in order of descending brightness, UH, CH, IP, CSH, voids and cracks) (Fig. 2b).

Scrivener and Pratt (1984) used similar arguments to distinguish phases within cement paste. However, the values of mean atomic number reported in the paper were incorrect. Scrivener and Pratt calculated the mean atomic numbers for phases within cement paste on the basis of the number of atoms instead of the weight fraction of the elemental components. This resulted in incorrectly predicting the mean atomic numbers and the

resulting relative intensities. The discrepancies are especially apparent for calcium hydroxide and the calcium silicate hydrates. Using their results, also shown in Table 2, the mean atomic number for calcium hydroxide, $\overline{Z}^* = 7.60$, lies within the mean atomic number range for CSH, $\overline{Z}^* = 7.10$ -- 8.20. This, however, is inconsistent with BSE images in which CH is always brighter than CSH. By comparing the two sets of mean atomic numbers shown in Table 2, it becomes evident that the Scrivener - Pratt values are low, especially for the hydration products. Approximate backscattering coefficients based on the mean atomic numbers given by Scrivener also are presented in Table 2.

Secondary Electrons

Secondary electrons are produced throughout the interaction volume as a result of inelastic scattering. Interactions between beam electrons and weakly bound conduction electrons transfer only a few electron volts of energy to the conduction band electrons and result in the emission of secondary electrons. Secondary electrons are defined as those electrons emitted from a sample with an energy less than 50 eV (Goldstein et al. 1981). Most secondary electrons do not escape from the sample material because of their low energy. Only those secondary electrons which are generated very close to the surface can emerge and be detected. Thus, secondary electrons have a very shallow sampling depth, approximately 10 nm, as shown in Fig. 1. Due to their shallow sampling depth, secondary electron signals carry only topographic information and do not provide atomic number contrast. As mentioned in the introduction, secondary electron images provide some atomic number information because some backscattered electrons reach the SED. However, this low BSE signal is generally not sufficient to distinguish phases based on atomic number.

X-ray Microanalysis

Characteristic and continuum x-rays are generated during the inelastic scattering process. Continuum x-rays are generated by the deceleration of beam electrons as they pass through the Coulombic fields near atomic nuclei. A continuous spectrum of x-ray energies is produced from zero up to the value of the incident electron energy. These x-rays are referred as continuum x-rays or bremsstrahlung (braking radiation). Characteristic x-rays are produced when a beam electron first ejects an inner-shell electron, leaving the atom in an ionized or excited state, followed by relaxation, as the atom returns to its original ground state. In the process of relaxation, electrons move from one shell to another, releasing energy in the form of x-ray photons. The energy of the photons is equal to the difference in the energy levels of the shells. Characteristic x-rays are thus sharply defined for each individual element. Fig. 3 shows a typical x-ray spectra for cement paste obtained with an energy dispersive spectrometer, EDS, mounted on a SEM. Each peak represents the energy of a characteristic x-ray of an element within cement paste.

Qualitative analysis of cement paste can be performed by using the energy dispersive spectrometer, EDS. Unhydrated cement particles have not reacted with water. Therefore, the concentration of oxygen in unhydrated materials will be lower than in hydration products. For example, two points, A and B are identified in the BSE image shown in Fig. 2a. Point A is located within a region having a high intensity and Point B is located within a region having a low intensity. Using the SEM in point mode, x-ray spectra are collected and presented in Figs. 3a and 3b for Points A and B, respectively. Comparing these two spectra, it can be seen that the oxygen Kα peak is lower in Fig. 3a than in Fig. 3b. Qualitatively, this shows that the oxygen concentration at point A is lower than the concentration at point B, providing supporting evidence that point A is located within an

unhydrated cement particle.

The EDS also can be used to identify calcium hydroxide, based on the absence of silicon. Fig. 4a is a silicon Kα x-ray dot map of the area shown in Fig. 2a. The regions of low intensity, i.e. low silicon concentration, show possible locations of calcium hydroxide (note, due to continuum x-rays, every point on the dot map is not necessarily due to the presence of silicon). Regions where C_4AF is present also have a low silicon concentration. To determine which regions contain C_4AF, iron Kα x-ray dot maps can be used to locate areas with high iron concentrations (as shown in Fig. 4b). By comparing Fig. 2a with Fig. 4, the locations and outline of calcium hydroxide within the image can be seen.

Iron Kα x-ray dot maps can also be used to differentiate phases within unhydrated materials. In x-ray dot maps, regions high in iron and low in silicon indicate the presence of C_4AF. Figs. 5 and 6 show the BSE image, and silicon and iron Kα x-ray dot maps of the same frame. In these figures, C_4AF and CH can be differentiated. C_4AF is high in iron and low in silicon, while CH is low in both iron and silicon. In the BSE image in Fig. 5, the C_4AF phase appears brighter than other unhydrated materials. This confirms the effect of the mean atomic number on a BSE image. From BSE images, the sequence of major phases within cement paste based on their intensities can be obtained, from bright to dark: 1) unhydrated materials including C_4AF, C_3S, C_2S, and C_3A 2) calcium hydroxide, 3) inner product, 4) calcium silicate hydrate, and 5) cracks and voids. This sequence of phases has the same order as the mean atomic numbers obtained using Eq. 3.

Continuum x-rays and characteristic x-rays are generated over a substantial fraction of the interaction volume. The following expression is used to predict the depth of x-ray production or x-ray generation range (Kanaya and Okayama 1972):

$$R_x = K(E_0^{1.67} - E_c^{1.67}) / \rho \qquad (6)$$

in which E_c is the critical ionization energy for an electron shell or the continuum energy of interest for continuum x-rays.

From the Kanaya-Okayama (1972) electron range (Eq. 1), K in Eq. 6 has a value of

$$K = 0.0276A / Z^{0.889} \qquad (7)$$

and thus depends on the target atomic number and weight. The x-ray generation range is shown schematically in Fig. 1.

Comparing the sampling volumes for different signals in Fig. 1, it becomes evident that secondary electrons have the least sampling depth, whereas x-rays have the largest sampling depth. Taking silicon with 25.0 keV acceleration voltage as an example, the backscattered electron interaction volume is R_{KO} = 6.85 μm (from Eq. 7), the sampling depth for backscattered electrons is $0.3R_{KO}$ = 2.04 μm, and the Si Kα x-ray generation range is R_x = 6.77 μm (from Eq. 8). It can be observed that x-rays carry information from a greater depth (6.77 μm) than do backscattered electrons (2.04 μm). The different sampling volumes affect not only the depth of information but the resolution obtainable from different signals. Since only secondary electrons produced near the point of beam impact can be detected, secondary electron images can have a high resolution, on the order of 4 nm or better. The larger sampling volumes for backscattered electrons and x-rays result in less resolution, typically 0.5 μm for BSE and 3 to 6 μm for x-rays.

Available Contrast

In an SE or BSE image, features are visible on the SEM because the intensity of signal changes from point to point. In a BSE image, for example, the signals from a high

atomic number material have a higher intensity than signals from a lower atomic number material, and thus appear brighter. The relative difference between signals, known as the contrast, C, can be obtained from the following equation:

$$C = \frac{\eta_1 - \eta_2}{\eta_1} \tag{8}$$

in which η_1 and η_2 are, respectively, the backscattering coefficients for the high and low density material.

A number of factors influence the contrast that can be observed on an SEM. The minimum level of contrast observable in an image is defined by the threshold equation (Oatley at el. 1965, Goldstein et al. 1981):

$$i_B > \frac{4 \times 10^{-12}}{\varepsilon C^2 t_f} \tag{9}$$

in which i_B is the minimum beam current required to provide contrast C, t_f is the time required to scan a 1000 x 1000 picture element (pixel) frame, and ε is the detector efficiency. The number in the numerator is proportional to the number of pixels in an image. For example, the image analysis system (IAS) used in this study has a pixel density of 512 x 480, reducing the numerator to about 1×10^{-12} for the same contrast available on the higher density pixel image. Since the slow scan speed on the IAS corresponds to $t_f = 32$ sec and the usual photographic scan speed on the SEM corresponds to $t_f = 128$ sec, roughly equal contrast is available on the two instruments. Eq. 9 is useful in determining if specific features can be imaged on an SEM.

Nonlinear Signal Processing

The images formed by an SEM are derived from the signal measurements. The original signals from the specimen have to be amplified to a suitable level by one or more amplifiers, so that the signals can be translated into a visible image. The quality or the visibility of the image displayed also depends on the output signal intensities and the contrast (the difference between signal intensities). The SEM can only display a limited range for output signal intensities. The signals which are near or exceed the upper and lower boundaries of the range will appear either white or black in the image and result in poor visibility. This is known as signal saturation. In some cases, the information carried by nearly saturated signals is desired. Then, nonlinear amplification (γ processing) can be applied.

Nonlinear amplification is a technique which processes the original input signals and provides selective contrast expansion at either the black or white end of the output signal intensity range. The signal response curve for nonlinear amplification is shown in Fig. 8. $\gamma = 0$ corresponds the linear amplification. For $\gamma > 1$, the dark end of the scale is expanded while the bright end is compressed; for $\gamma < 1$, the reverse is true.

Application of Image Analysis System

The image analysis system (IAS) can be used for feature identification and quantitative analysis of images obtained from the SEM. The IAS has the ability to distinguish 256 gray levels, dark to bright, ranging from 0 to 255, at a density of 512 x 480 picture elements (pixels) on the monitor. When an image is transferred from the SEM to the IAS, pixels with gray levels representing the signal intensities from corresponding points on the specimen form the image on the monitor. The IAS used in this study can

divide the pixels into up to 15 groups based on gray level. This is referred to as creating thresholds for gray level ranges. This allows the area and shape of a group of pixels with like intensity gray levels to be identified. Quantitative analysis can be carried out on these thresheld regions.

EXPERIMENTAL PROGRAM

Cement Paste

The cement paste specimens used in this study were prepared with Type I portland cement at a water-cement ratio of 0.4 and cured for 28 days in lime saturated water at 72 °F.

Preparation of the Standard

A two-material standard was prepared for this research. The standard consists of a thin silicon wafer (100 μm) mounted on a piece of polished magnesium (10x10x7 mm). The silicon wafer is mounted on the magnesium using cyanoacrylate adhesive (super glue).

To prepare the standard, the magnesium was polished by hand using silicon carbide (SiC) paper, starting with 320 grade and proceeding to 600, 1000, and 2000 grades. Polishing with diamond paste followed, proceeding from 3 μm to 1 μm to 0.5 μm paste. The surface was thoroughly cleaned after each stage of polishing with a lint free cloth and a commercial compressed gas cleaner.

The standard was mounted on an aluminum specimen stub, and colloidal graphite was used to provide electrical conductivity between the silicon, the magnesium, and the specimen stub.

Although a thinner layer of silicon would have worked as well, the 100 μm wafer served the purpose quite well. A change of 100 μm in free working distance is beyond the sensitivity of the SEM because of the high depth of field inherent in the instrument. The SEM is able to detect a change in the FWD of approximately 0.5 mm or 500 μm, which is much greater than the thickness of the silicon wafer. Therefore, the SEM can focus on the magnesium and the silicon simultaneously.

The interaction volume for silicon is fully contained within the wafer. Using an accelerating voltage of 25.0 keV, the interaction volume for silicon is R_{KO} = 6.8 μm (Eq. 7). This is far less than the 100 μm thickness of the silicon and insures that beam electrons will not break through the silicon wafer and produce BSE signals with mixed information. The values of Z, A, and η for magnesium and silicon are summarized in Table 3.

Specimen Preparation

In preparing specimens for the scanning electron microscope, cement paste specimens were sectioned into 1 mm thick segments with a high speed diamond saw. The specimens were oven dried at 105 °C for 24 hours and held in a desiccator cabinet until the time for further processing.

Specimens were impregnated with an ultralow viscosity epoxy prior to imaging in the SEM. Epoxy provides support for the cement microstructure, prevents damage during polishing, and keeps polishing material out of the cracks and voids. Because of its low mean atomic number, cracks and voids appear black in a BSE image of cement paste. A vacuum saturation technique was used for epoxy impregnation. The specimens were first subjected to a low level vacuum (50 torr.). Epoxy was drawn into the chamber under

vacuum pressure, and then normal pressure was restored. The epoxy was polymerized at 60 °C for 24 hours.

Following polymerization, specimens were polished by hand using progressively finer grades of silicon carbide (SiC) paper and diamond paste. Polishing started with 320 grade SiC paper, proceeding to 600, 1000, and 2000 grades; followed by 3 μm, 1 μm, and 0.5 μm diamond polishes. After each stage of polishing, the specimen surface was carefully cleaned with a dry lint free cloth and a commercial compressed gas cleaner.

A jig was used to insure the specimens and the standard would be the same height (7 mm). This is particularly useful for multiple sample studies. A piece of teflon was placed at the bottom of the jig to protect the polished specimen surface. After polishing the viewing surface up to 1000 grade SiC paper, the specimens were placed, viewing surface down, in the jig and ground down to the level of the surface of the jig. Polishing then continued with 2000 grade SiC paper. Since the grain size of 2000 grade SiC paper is 3 μm, polishing with 2000 grade paper and the diamond paste does not cause a sizable change in specimen height.

During polishing, it was found to be important that some epoxy be left covering the viewing surface of the specimen following polishing with 600 grade paper, because coarse sand paper leaves deep scratches on the specimen surface. It is better to have these scratches in the epoxy than in the cement paste. Ideally, the thin layer of epoxy remaining on the viewing surface should be removed with the 1000 and 2000 grade paper.

After 2000 grade SiC paper grinding was complete, specimens were polished with diamond paste on a piece of non-scratched glass. Although the grain size of 2000 grade SiC paper is 3 μm, it was observed, using the light microscope, that because the grains are glued together, the actual particle size is greater than 3 μm. Therefore, polishing started

with 3 μm diamond paste and proceeded to 1 μm, and 0.5 μm paste.

Surface cleaning between each grinding and polishing stage was done with care. After each stage, specimens were carefully and completely cleaned with a dry lint free cloth and a commercial compressed gas cleaner. A dry cloth was used rather than a solvent to prevent the dissolution of any constituents. A different cleaning cloth was used for each stage of polishing to prevent larger particles from contaminating the surface and causing severe scratches. This was especially important when polishing with diamond paste. Polishing was done slowly and with minimal pressure applied to the specimen in order to prevent deep scratches from occurring. Normally, it took about 10 minutes for each step with the 1000 and 2000 grade papers and the three diamond pastes. When polishing with 0.5 μm diamond paste was complete, any diamond paste residue was removed by wetting a cloth with a few drops of ethanol and quickly cleaning the specimen surface. Care had to be taken because the epoxy is soluble in ethanol.

A light microscope was used to determine when specimens were properly polished, up through use of the 2000 grade paper. Specimens were coated with 10 nm of gold-palladium in a sputter coater and were observed through a light microscope. The gold-palladium coating increased the visibility of scratches on the cement surface under the light microscope. The specimen was temporarily mounted on an aluminum stub, and the SEM was used for a closer check. At 1010x and with secondary electron imaging, the width of scratches could be measured. This provided an accurate method to control the sample preparation quality.

After polishing was complete, specimens were mounted on aluminum stubs and coated with a 20 nm layer of gold-palladium in the sputter coater. Upon completion of these procedures, the specimens were ready for imaging in the SEM.

cracks and voids are difficult to discern in this image. Fig. 11b is the same image with γ processing, $\gamma > 1$. The details in the CSH structure are much clearer.

Image Analysis System Calibration followed BSD calibration. Calibration of the IAS with mean SEM signal intensities of -3 (Si) and -15 (Mg) is described below. The procedure for signal intensities of -8 (Si) and -18 (Mg) is similar.

IAS calibration started with a BSE image of the standard at 300x. The contrast and brightness on the BSD were adjusted to mean Si/Mg signal intensities of -3/-15. The image was then acquired by the IAS at the minimum scan speed (frame time = 32 sec.) and the maximum contrast setting (gain = 10) on the IAS. The signal intensity on the IAS was adjusted so that the peak signal intensity for Si corresponded to the horizontal center line of the IAS videoscope. This gave a good first approximation for the desired settings on both the SEM and the IAS.

A pseudo-color gray level threshold file was used to verify that the system was properly calibrated. As described in the Background section, the IAS has the ability to distinguish 256 gray levels, ranging from 0 to 255. These digitized gray levels were used to represent the signal intensities of the image. In a threshold file, a single color can be assigned to a range of gray levels. The IAS allows up to 15 ranges or thresholds for one image. Each gray level range can be represented by a distinct user-defined pseudo-color. The threshold file used for the Si-Mg standard (Table 4) used red to represent the gray levels of Si, ranging from 102 to 138, and blue to represent the gray levels of Mg, ranging from 24 to 62. Yellow and purple were used for the gray levels above silicon and for the gray levels between Si and Mg, respectively. Black represented gray levels below 24.

A color image of the standard was obtained by executing the pseudo-color threshold file. With the IAS properly calibrated, the color image showed a virtually solid red section

for silicon and a solid blue section for magnesium, with a black strip running along the Si-Mg interface (the vertical surface produced few BSE in the direction the detector). The image contained some discrete spots of yellow where gray levels were higher than those for silicon, and spots of purple where gray levels were between those of silicon and magnesium. These spots were caused by 1) imperfections in the sample surface due to sample preparation, and 2) signal noise due to the nature of the SEM. When the system is properly set, the total area of the yellow phase and the total area of the purple phase should each be approximately 1 percent of the total frame area.

Once the pseudo-color image of the standard was obtained, the SEM and IAS were properly calibrated. If calibration had not been obtained, as indicated by the threshold file, then the contrast and brightness on the BSD and the settings on the IAS, were again readjusted. These steps were repeated until calibration was obtained.

A stable beam current during image acquisition is crucial because a variation in beam current will change the contrast and brightness of an image. For that reason, beam current was checked periodically and the SEM, BSD and IAS adjusted as required.

The procedure described above was also used when calibrating the system for videoscope settings of -8 (Si) and -18 (Mg). The gray level threshold file for this calibration, however, is different from the threshold file used above, as shown in Table 5. Gray levels for silicon range from 146 to 188 and gray levels for magnesium range from 27 to 97.

X-ray Dot Mapping was used as an alternative method to distinguish phases within cement paste. However, a direct EDS x-ray dot map image on the SEM is rarely satisfactory for pinpointing concentrations of specific elements within cement. This is because continuum x-rays reduce the resolution of EDS; hence, x-ray dot maps do not

show distinct concentrations of characteristic x-rays. It is possible to superimpose multiple x-ray dot maps of a region on the same micrographs. However, due to the gray scale setting on the SEM, the non-zero intensities of the background for each superimposed micrograph are also accumulated and the gray background of the micrograph becomes brighter as each new image is added. Therefore, only a limited number of x-ray dot map micrographs can be superimposed, and the resulting image is still not of good quality.

To improve the quality of an x-ray dot map, the IAS can be used together with the SEM and the EDS. After accumulating a number of x-ray dot map images on the IAS, the resulting image can be adjusted by subtracting a number of gray levels to insure that the background is at 0 gray level. This is followed by multiplication by a large number, making the remaining non-zero pixels reach or exceed a gray level of 255, while the background remains 0. Since 255 and 0 are the upper and lower saturation limits on the IAS, signals with intensities greater than 255 remain at 255 and those with intensities of 0 remain 0.

Figs. 5 and 6 show the x-ray dot maps taken using the IAS. Each x-ray dot map is the accumulation of 50 direct images at the minimum scan speed (frame time = 32 sec.) and the maximum contrast (gain = 10) on the IAS. Gray levels were adjusted every five images by subtracting 70 and then multiplying by 20. An "autocontrol" file on the IAS was created so that the process could be done automatically.

Image analysis of cement paste was carried out following calibration of the SEM and IAS. Cement paste specimens were viewed at a FWD = 25.5 mm and magnifications of 503x or 1010x. Images were transferred from the SEM to the IAS for analysis. A pseudo-color gray level threshold file was created for the gray level ranges of the phases within cement paste, as listed in Table 6. The five gray level ranges representing the five

major phases within cement paste are 1) 212 to 255 for unhydrated cement particles, 2) 159 to 211 for calcium hydroxide, 3) 107 to 158 for non-calcium hydroxide inner product, 4) 16 to 106 for calcium silicate hydrate and 5) 0 to 15 for cracks and voids. An BSE image and the corresponding pseudo-color image are presented in Fig. 12.

Once the gray levels corresponding to the individual phases were established, the percent area for each of the phases could be determined. The procedure consisted of collecting a series of BSE images at evenly spaced intervals across the specimen. Each image was transferred from the SEM to the IAS and the percent area of each phase in the image was determined using the threshold file on the IAS. The IAS can also provide an analysis of feature size, shape, and orientation, as will be later discussed.

RESULTS AND DISCUSSION

The Standard And Its Materials

The BSE imaging techniques used by other researchers (Scrivener and Pratt 1984, Scrivener et al. 1985, Scrivener and Gartner 1988, Scrivener 1989, Kjellsen et al. 1990) are valid for the qualitative analysis of cement-based materials. However, if quantitative information is required, these techniques have the disadvantage that the intensity of identical phases may change each time the SEM and the IAS are set up. These differences in signal intensity can be adjusted by the operator; however, the adjustment is both subjective and impractical for a statistical analysis for studies in which hundreds of frames are required. Variations in signals are more noticeable when the images are transferred to the IAS than on the SEM alone, since the IAS is able to distinguish 256 different gray levels and is thus more sensitive to changes in intensity.

The procedures described in this report were developed to help insure that the phases within cement paste can be recognized consistently. Two materials with different mean atomic numbers are necessary to allow both contrast (difference in signals) and brightness (magnitude of signals) to be established. To be most effective, a standard must possess atomic numbers that are within the range of the materials being imaged. For cement paste, the mean atomic numbers for major constituents range from 10.76 to 16.65, as shown in Table 2. The standard materials should also be chemically stable. Silicon (atomic number 14) and magnesium (atomic number 12) meet these requirements.

Based on the threshold equation (Eq. 3), under operating conditions of $1x10^{-9}$ amps beam current, 128 second frame time and 25 percent detector efficiency, the lower limit of contrast on the SEM is 1.1 percent. [Note. This means that although not attempted in this study, BSE imaging on the SEM should be able to differentiate between C_3A (η = 0.1639) and CH (η = 0.1618) at a contrast of 1.3 percent.] The contrast between the two standard materials is 14.1 percent, as calculated by Eq. 2, and is on the same order as the contrast available from cement paste. Thus, silicon and magnesium satisfy both contrast and intensity requirements for imaging cement paste.

In the current study, two videoscope settings were used depending on the information desired. Mean signal intensities of -3 for silicon and -15 for magnesium on the arbitrary videoscope scale proved best for differentiating the five major phases within cement paste. Mean signal intensities of -8 for silicon and -18 for magnesium were best if details of phases within the unhydrated cement particles are desired.

The -3/-15 setting uses the full intensity range possible on both the SEM and the IAS. The major purpose of using this setting is to gain the maximum contrast between the five major phases by treating the unhydrated materials as a single phase while obtaining clear

images for feature analysis. With this setting, the intensities of high mean atomic number particles, such as C_4AF, exceed the upper limit of the intensity range on both the SEM and the IAS. The gray level ranges for the standard corresponding to this setting are presented in Table 4. The gray level ranges for the phases in cement paste are presented in Table 6.

The -8/-18 setting can be used if detailed information on the unhydrated materials is desired. This setting can be used to effectively distinguish the phases within the unhydrated cement particles. Because of the lower effective intensity and image contrast produced with this setting, less information is available on low intensity features. Standard gray level ranges for this setting are presented in Table 5.

BSE images obtained with -3/-15 and -8/-18 two settings are compared in Fig. 13. Note the difference in detail provided for phases within the unhydrated cement particles.

In a recent article, Scrivener (1989) reported that the unhydrated materials and calcium hydroxide within cement paste have fairly uniform gray levels, which was explained by two sharp peaks in a histogram of the gray level distribution. During the current study, it was observed that both unhydrated materials and calcium hydroxide had fairly wide ranges of gray level, as shown in Table 6. By using a histogram of the gray level distribution obtained in this study, three peaks, representing unhydrated materials, calcium hydroxide and calcium silicate hydrate were obtained (Fig. 14). However, the peaks for the unhydrated particles and calcium hydroxide shown in Fig. 14 are broader than those obtained by Scrivener (1989). In comparison, Fig. 15 was taken with the IAS contrast reduced by 25 percent. The peaks become sharper as the contrast on the IAS is reduced. This experiment shows that a change in the contrast settings on the IAS can change the appearance of the histogram because lower contrast tends to compress the gray level range on the IAS and reduce the horizontal dimension of the histogram so that the peaks look

sharper, suggesting a uniform gray level for specific phases. However, an image with reduced contrast provides reduced efficiency for phase identification and quantitative analysis.

Phases of Inner Product and Calcium Silicate Hydrate

Inner product is the hydration product that forms within the original boundary of the cement grain. If unhydrated materials are considered as a single phase, inner product is the third brightest phase in a BSE image. Typically, inner product is observed adjacent to regions of unhydrated cement (Fig. 2b), but may appear independently if the specimen surface is just above or below a cement particle.

A number of investigations have found that inner product always forms around C_3S (Brown and Carson 1936, Williamson 1972, Stucke and Majumdar 1976). This is also observed in this study, as shown in the x-ray dot maps (Fig. 4), where the material adjacent to inner product is high in silicon and low in iron (really just continuum radiation with energy of Fe Kα x-rays). By combining iron and silicon x-ray dot maps a BSE image, and using the IAS to check the gray level, it is noted that no inner product appears around C_4AF unhydrated particles (the particles with the high iron concentration).

Since inner product results from the hydration of C_3S, both CH and CSH should be visible within this region. The existence of calcium hydroxide within inner product can be observed using thin sections in a transmission electron microscope (Dagleish et al. 1980, Dagleish and Ibe 1981) and in secondary electron images of fractured surfaces. Figs. 16 and 17 are micrographs of a fractured surface. Figs. 16a and 16b show a unhydrated particle surrounded by hydration products. Typical calcium hydroxide crystals can be seen adjacent to the unhydrated particle. Point mode x-ray analysis on the particle shows a

spectrum with a relatively high silicon Kα peak and the absence of an iron peak, indicating that the particle is calcium silicate. Figs. 17a and 17b show another example, this time of a "shell" structure of inner product where an unhydrated particle has been removed. Typical CH crystals can also be observed.

BSE images from the IAS also give evidence of calcium hydroxide within inner product. When the images are transferred from the SEM to the IAS, the system distinguishes the phases based only upon intensity (gray level), which, in turn, depends on mean atomic number. In this study, a significant portion of inner product appears to have the same signal intensity as observed for massive regions of calcium hydroxide. Fig. 12 shows both original and thresheld BSE images. Massive calcium hydroxide particles and portions of inner product have the same gray level.

The BSE intensity of the CSH within inner product is higher than the intensity of the CSH that forms outside of the original boundary of the cement grain. This allows these two hydration products to be distinguished from each other. This also suggests that the CSH within inner product has a denser structure.

The fact that inner product is formed around the particles of C_3S, but not C_2S, is illustrated in Figs. 11 and 12. Each figure, shows two prominent unhydrated cement grains, one of which is surrounded by inner product and one of which is not. EDS analysis showed that both grains in each figure consisted of calcium silicates. The grains without inner product appear slightly darker than the grains with inner product as would be predicted based on the slightly lower backscattering coefficient of C_2S (Table 2).

The existence of calcium hydroxide within inner product cannot be observed with the EDS on the samples used in this study because the x-ray generation range is deep enough to pick up silicon in all but massive deposits of calcium hydroxide. The mean atomic

numbers for calcium hydroxide and calcium silicate hydrate are 14.30 and 12.39, respectively. The x-ray generation range for calcium hydroxide is 6.1 μm at 25.0 keV (Eq. 6). Thus, the depth of a calcium hydroxide crystal must be on the order of 6.1 μm for an x-ray dot map to show a low concentration of silicon, and calcium hydroxide within inner product cannot be verified using the EDS.

Number of Frames Required for Image Analysis

Data on phases within hydrated cement is obtained at locations across a specimen. A minimum number of frames is required to provide a level of statistical confidence in the results. The number of frames, n, required for 95 percent confidence that the area percent of a phase is within ε of the true average is given by

$$n = \left(\frac{1.96 \times \sigma}{\varepsilon} \right)^2 \qquad (10)$$

in which n is the estimated sample size necessary for the desired precision and confidence, σ is the preliminary estimate of the population standard deviation of the area percent for a phase, and ε is the acceptable error or half of the maximum acceptable confidence interval (Ostle and Malone, 1988). The sample size, n, increases as the allowable error, ε, decreases, and as the variability in the population, as denoted by σ, increases.

To obtain data on the test sample and determine the number of frames required, 230 frames and 80 frames, respectively, were analyzed at magnifications of 1010x and 503x. Tables 7 and 8 provide the results of the analysis, including percent area, minimum number of frames, n, and the corresponding total sampling area required for each phase at each magnification to provide 95 percent confidence that the results are within 10 percent of the

measured value. The material identified as inner product, represents the non calcium hydrate portion of the phase. CH from all regions is identified as a single phase.

Tables 7 and 8 show that the number of frames required decreases as the magnification decreases, but that the total sampling area increases as the magnification decreases. For example, at a magnification of 1010x, a minimum of 153 frames is required for unhydrated cement particles, with a corresponding area of 9.11×10^6 μm^2. At a magnification of 503x, the same phase requires only 64 frames but a corresponding area of 1.54×10^7 μm^2. This phenomenon, known as the "scale effect" has been noticed in other image analysis applications (Serra 1982).

One reason for this phenomenon is related to the resolution of the IAS. The size of a pixel is a fixed portion of the viewing area. Thus, the area represented by a single pixel varies with the magnification. At a magnification of 500x, a pixel represents four times the area of a pixel at 1000x. The effect is to reduce the clarity of boundaries between phases as the magnification is decreased. Since the gray level of a pixel on a boundary will be the average of the gray levels from two phases, the IAS must assign that pixel based on an intensity that does not accurately represent either phase. Depending on the grey level ranges assigned to individual phases, the pixel may be assigned to one of the adjacent phases or even to a third phase. Therefore, as magnification is lowered, the system tends to lose detailed information about features. This leads to an increase in the scatter in the percent area for a phase.

From Tables 7 and 8 it can also be noted that to achieve a desired level confidence, the number of frames required for each phase is different. At a magnification of 1010x, 153 frames are required for unhydrated cement particles, compared to 23 frames for calcium hydroxide, 7 frames for inner product and calcium silicate hydrate, and 71 frames

for cracks and voids. Note that unhydrated cement particles require the greatest number of frames, while calcium silicate hydrate and inner product require the least. The same tendency is apparent for the results obtained at a magnification of 503x, as shown in Table 8.

CONCLUSIONS

The following conclusions are based on the experimental work and analyses presented in this report.

1. Silicon and magnesium possess backscattered electron coefficients which are within the range of the backscattered electron coefficients of the phases within hydrated cement paste.

2. A silicon-magnesium standard can be used to establish an objective method for setting both a scanning electron microscope and an image analysis system for backscattered electron imaging of hydrated cement paste.

3. Backscattered electron imaging of polished surfaces of epoxy impregnated cement paste can be used to distinguish calcium silicates and calcium aluminoferrite within unhydrated particles, and calcium hydroxide, calcium silicate hydrate within inner product, calcium silicate hydrate outside of the original cement grain boundaries, and cracks and voids.

4. The existence of calcium hydroxide within inner product can be confirmed by secondary electron imaging of fractured surfaces and backscattered electron imaging of polished surfaces.

5. Material identified as inner product consists of the hydration products of tricalcium

silicate C_3S.

6. Scanning electron microscope x-ray dot maps do not provide information on calcium hydroxide within inner product. This is due to a large x-ray generation range compared with the volume of inner product.

7. For image analysis, the number of frames required for a selected level of confidence decreases as the magnification decreases, while the total area required increases as the magnification decreases. This is due to the scale effect.

8. To achieve a desired level of confidence in image analysis for the phases of hydrated cement paste, unhydrated cement particles require the greatest number of frames, while inner product and calcium silicate hydrate require the least number of frames.

ACKNOWLEDGEMENTS

This report is based on research performed by Hong Zhao in partial fulfillment of the requirements for the MSCE degree from the University of Kansas. This research was supported by the Air Force Office of Scientific Research under Grant AFOSR-89-0296.

REFERENCES

Attiogbe, E. K. and Darwin, D. (1985). "Submicroscopic Cracking of Cement Paste and Mortar in Compression," *SM Report* No. 16, University of Kansas Center for Research, Lawrence, November, 439 pp.

Attiogbe,e. and Darwin, D. (1987). "Submicrocracking in Cement Paste and Mortar," *ACI Materials Journal*, Vol. 84, No. 6, November-December, pp.491-500

Barker, A. P. and Barnes, P. (1984). "A Review of Techniques for Phase Delineation within Cement in the Scanning Electron Microscope," *Proceedings*, 6th International Conference on Cement Microscopy, Albuquerque, pp. 156-172

Barnes, P., Fonseka, G. M., Ghose, A. and Moore, N. T. (1979). "Ion Beam Etching in the Study of Cementitious Materials," *Journal of Materials Science*, vol. 14, No. 12, December, pp. 2831-2836

Barnes, P., Jeffery, J. W. and Sarkar, S. L. (1978). "Composition of Portland Cement Belites," *Cement and Concrete Research*, Vol. 8, No. 5, September, pp. 559-564

Brown, L. S. and Carlson, R. W. (1936). "Petrograghic Studies of Hydrated Cement," *Proceedings*, American Society for Testing and Materials, vol. 36, pp. 332-350

Dalgleish, B. J. and Pratt, P. L. (1982). "Fractographic Studies of Microstructural Development in Hydrated Portland Cement," *Journal of Materials Science*, Vol. 17, No. 8, August, pp. 2199-2207

Dalgleish, B. J. and Ibe, K. (1981) "Thin-Foil Studies of Hydrated Portland Cement," *Cement and Concrete Research*, Vol. 11, No. 5/6, September/November, pp. 729-739

Dalgleish, B. J., Pratt, P. L. and Moss, R. I. (1980). "Preparation Techniques and the Microscopical Examination of Portland Cement Paste and C_3S," *Cement and Concrete Research*, Vol. 10, No. 5, September, pp. 665-676

Diamond, S. (1976) "Cement Paste Microstructure -- An Overview of Several Levels," *Proceedings*, Conference on Hydraulic Cement Pastes: Their Structure and Properties, Cement and Concrete Association, University of Sheffield, England, April, pp. 2-30

Goldstein, I., Newbury, D., Echlin, P., Joy, D., Fiori, C.and Lifshin, E. (1981). *Scanning Electron Microscopy and X-Ray Microanalysis*, Plenum Press, New York and London, 673 pp.

Heinrich, K. F. J. (1966). "X-Ray Optics and Microanalysis," *Proceedings*, 4th International Congress on X-Ray Optics and Microanalysis, eds. R. Castaing, P. Deschamps, and J. Philibert, Hermann, Paris, pp. 1509

Jennings, H. M. and Pratt, P. L. (1980). "The Use of a High-Voltage Electron Microscope and Gas Reaction Cell for the Microstructural Investigation of Wet Portland Cement," *Journal of Materials Science*, Vol. 15, No. 1, January, pp. 250-253

Kanaya, K. and Okayama, S. (1972). "Penetration and Energy-Loss Theory of Electrons in Solid Targets," *Journal of Physics. D: Applied Physics*, Vol. 5, No. 1, January, pp. 43-58

Kjellsen, K., Detwiler, R., and Gjørv, O. (1990). "Backscattered Electron Imaging of Cement Pastes Hydrated at Different Temperatures," *Cement and Concrete Research*, vol. 20, No. 2, March, pp. 308-311

Oatley, C. W., Nixon, W. C., and Pease, R. F. W. (1965). In *Advances in Electronics and Electron Physics*, ed. L. Marton, Academic, New York, pp. 181

Ostle, B. and Malone, L. C. (1988). *Statistics in Research*, Iowa State University Press, Fourth Edition, 649 pp.

Scrivener, K. L. (1989). "The Use of Backscattered Electron Microscopy and Image Analysis to Study the Porosity of Cement Paste," *Material Research Society Symposium Proceedings*, Vol. 137, pp. 129-140

Scrivener, K. L., Baldie, K. D., Halse, Y. and Pratt, P. L. (1985). "Characterization of Microstructure as a Systematic Approach to High Strength Cements," *Material Research Society Symposium Proceedings*, Vol. 42, pp. 40-43

Scrivener, K. L. and Gartner, E. M. (1988). "Microstructural Gradients in Cement Paste around Aggregate Particles," *Material Research Society Symposium Proceedings*, Vol. 114, pp. 77-85

Scrivener, K. L. and Pratt, P. L. (1984). "Backscattered Electron Images of Polished Cement Sections in the Scanning Electron Microscope," *Proceedings*, 6th International Conference on Cement Microscopy, Albuquerque, pp. 145-155

Serra, J. (1982) *Image Analysis and Mathematical Morphology*, Academic Press, 601 pp.

Struble, L. and Byrd, E. (1986) "Epoxy Impregnation of Hardened Cement Pastes for Characterization of Microstructure," Progress Report, NBSIR 87-3504, November, 9 pp.

Struble, L. and Stutzman, P. (1988) "Epoxy Impregnation Procedure for Hardened Cement Samples," NBSIR Report, February, 24 pp.

Stucke, M. S. and Majumdar, A. J. (1976). "The Composition of the Gel Phase in Portland Cement Paste," *Proceedings*, Conference on Hydraulic Cement Pastes: Their Structure and Properties, Cement and Concrete Association, University of Sheffield, England, April, pp. 31-54

Williamson, R. B. (1972) "Solidification of Portland Cement," Progress in Materials Science, Vol. 15, No. 3., May, pp. 189-286

Table 1. Atomic numbers, atomic weight and backscattering coefficient of major chemical components within portland cement

Element	Atomic Number Z	Atomic Weight A	Backscattering Coefficient η
H	1	1.008	0.0
O	8	16.00	0.0911
Al	13	26.98	0.1530
Si	14	28.09	0.1644
S	16	32.06	0.1864
Ca	20	40.08	0.2268
Fe	26	55.85	0.2795

Table 2. Mean atomic numbers and backscattering coefficients of major constituents in portland cement and their hydration products

Phases	Mean Atomic Number $\bar{Z}$	$\bar{Z}$*	Backscattered Coefficient $\eta_{mix} = \sum_i C_i\eta_i$	$\eta_{mix}(\bar{Z}^*)$
C_3S	15.06	12.67	0.1716	0.1491
C_2S	14.56	12.29	0.1662	0.1447
C_3A	14.34	12.18	0.1639	0.1434
C_4AF	16.65	13.22	0.1860	0.1555
CH	14.30	7.60	0.1618	0.0858
$CSH_{1.5}$	12.39	7.10	0.1413	0.0791
$C_{1.5}SH_2$	12.78	8.20	0.1455	0.0938
$C_3AS_3H_{32}$ (ettringite)	10.76	5.26	0.1233	0.0537
C_3ASH_{12} (monosulphate)	11.66	6.08	0.1328	0.0652

* Results from Scrivener and Pratt (1984)

Table 3. Atomic numbers, atomic weight and backscattering coefficients of standard materials

Element	Atomic Number Z	Atomic Weight A	Backscattering Coefficient η
Mg	12	24.31	0.1412
Si	14	28.09	0.1644

Table 4. Silicon-Magnesium Standard Gray Level Threshold Setting (Silicon / Magnesium = -3 / -15)

Level No.	Phase	Gray Level (Low)	Gray Level (High)
1		139	255
2	Si	102	138
3		63	101
4	Mg	24	62
5		0	23

Table 5. Silicon-Magnesium Standard Gray Level Threshold
(Silicon / Magnesium = -8 / -18)

Level No.	Phase	Gray Level (Low)	Gray Level (High)
1		189	255
2	Si	146	188
3		98	145
4	Mg	27	97
5		0	26

Table 6. Cement Paste Gray Level Threshold Setting
(Silicon / Magnesium = -3 / -15)

Level No.	Phases	Gray level (Low)	Gray level (High)
1	UH	212	255
2	CH	159	211
3	IP(CSH)	107	158
4	CSH	16	106
5	Cracks & Voids	0	15

Table 7. Area percent analysis of 28-day old cement paste including the number of frames required for 95 percent confidence that the area percent is within 10 percent of the measured value - 1010x Magnification

Phases	Percent Area %	Standard Deviation σ	Number of Frames Required n	Corresponding Area Required (μm^2)
UH	10.123	6.385	153	9.11×10^6
CH	15.637	3.899	23	1.36×10^6
IP(CSH)	22.830	3.087	7	4.16×10^5
CSH	44.391	5.840	7	4.16×10^5
Cracks & Voids	6.979	3.006	71	4.23×10^6

Table 8. Area percent analysis of 28-day old cement paste including the number of frames required for 95 percent confidence that the area percent is within 10 percent of the measured value - 503x Magnification

Phases	Percent Area %	Standard Deviation σ	Number of Frames Required n	Corresponding Area Required (μm^2)
UH	10.400	4.24	64	1.54×10^7
CH	15.577	3.11	16	3.84×10^6
IP(CSH)	22.011	1.98	4	9.60×10^5
CSH	44.153	4.21	4	9.60×10^5
Cracks & Voids	7.860	3.12	61	1.46×10^7

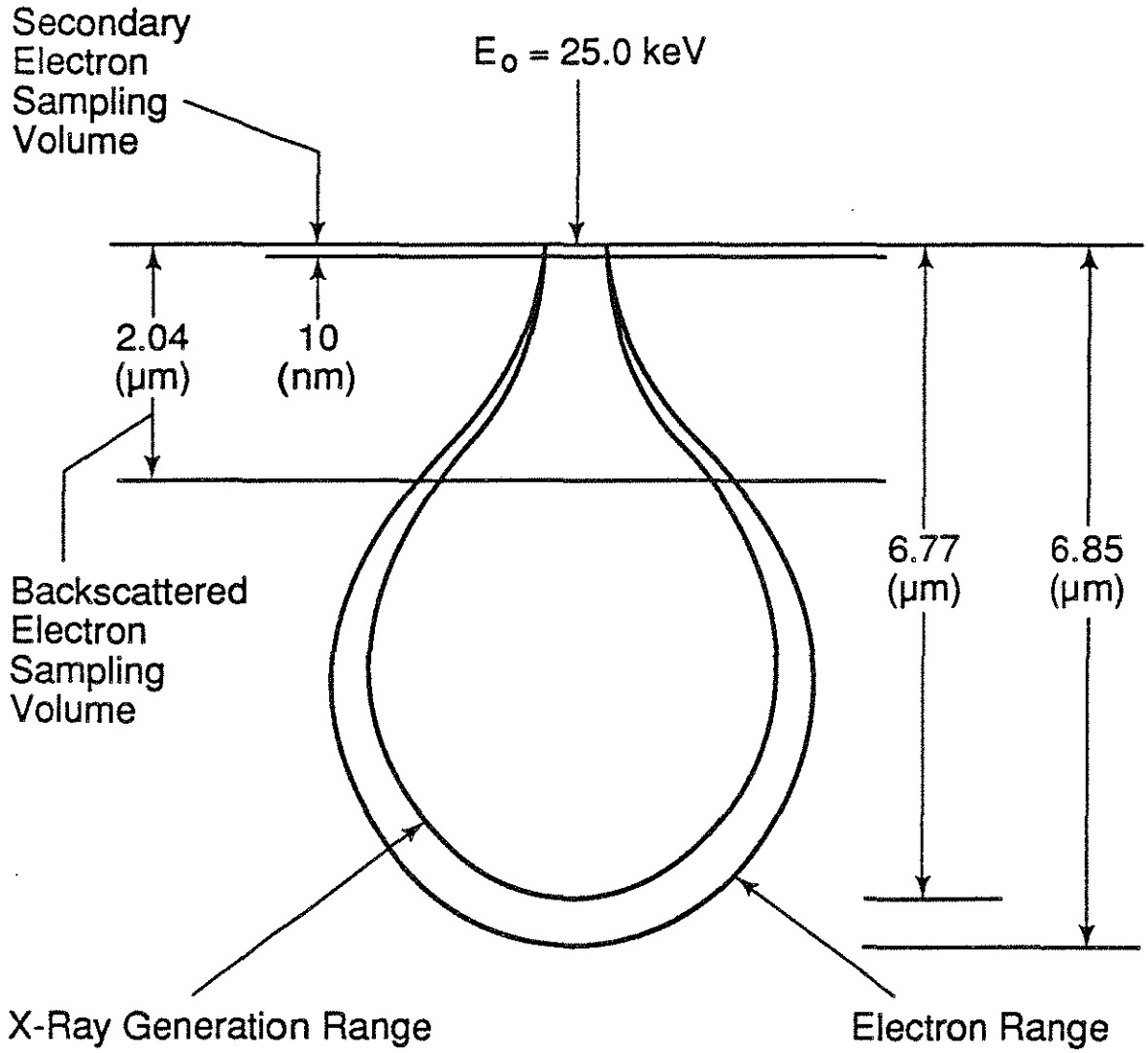

Fig. 1 Interaction volumes and sampling volumes for Si, E_0 = 25.0 keV.

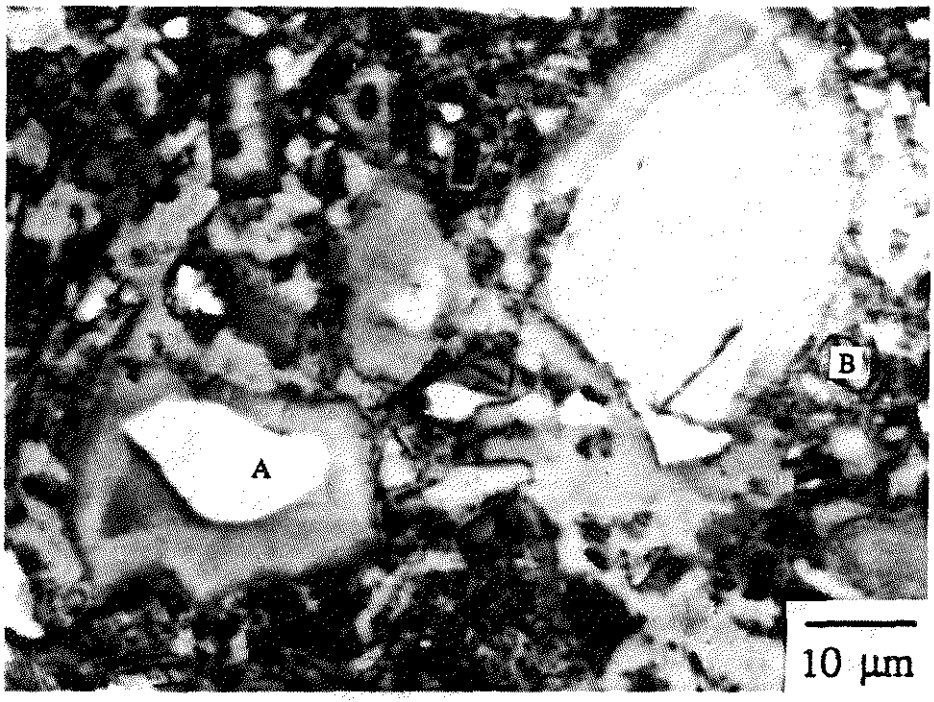

Fig. 2a BSE image of hydrated cement paste. W/C = 0.4. Age = 28 days.

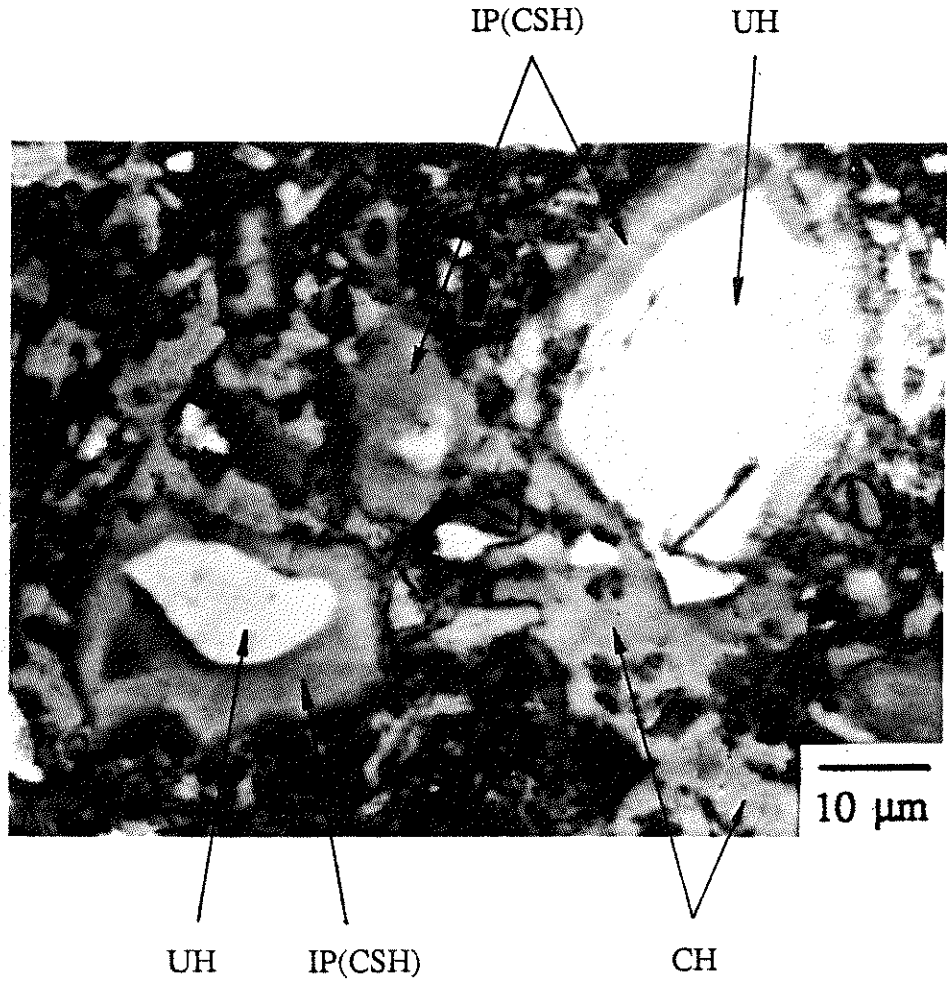

Fig. 2b Phases in Fig. 2 identified by their intensities

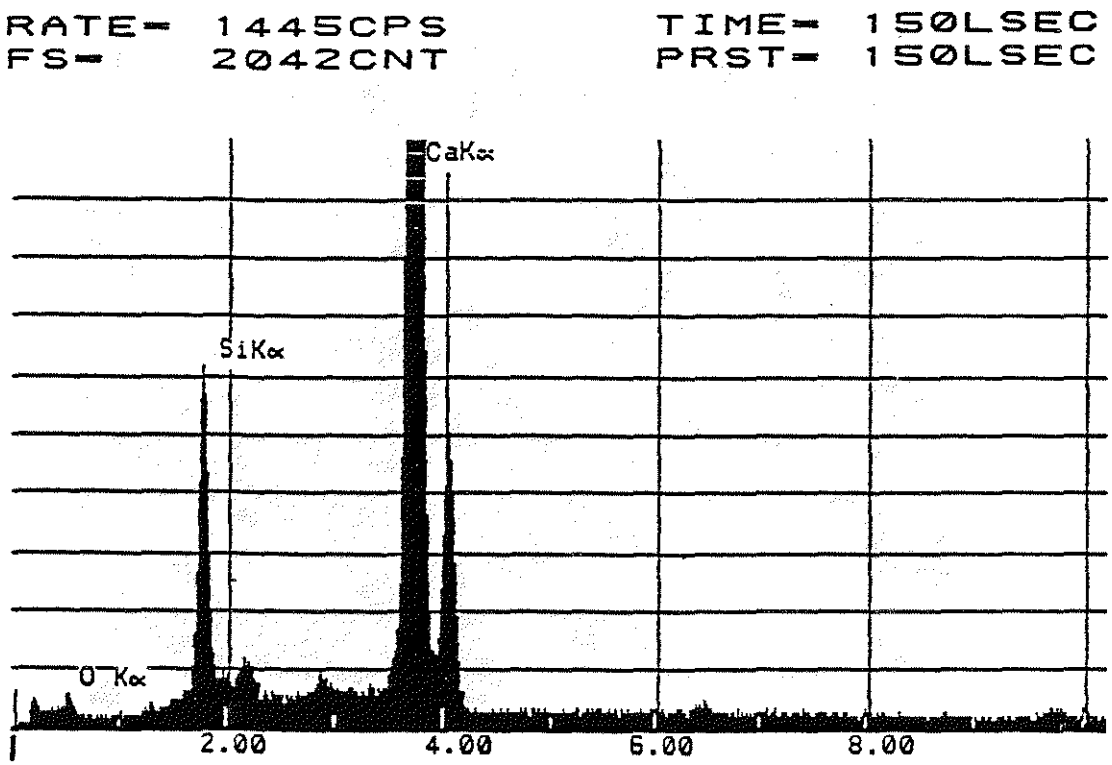

(a)

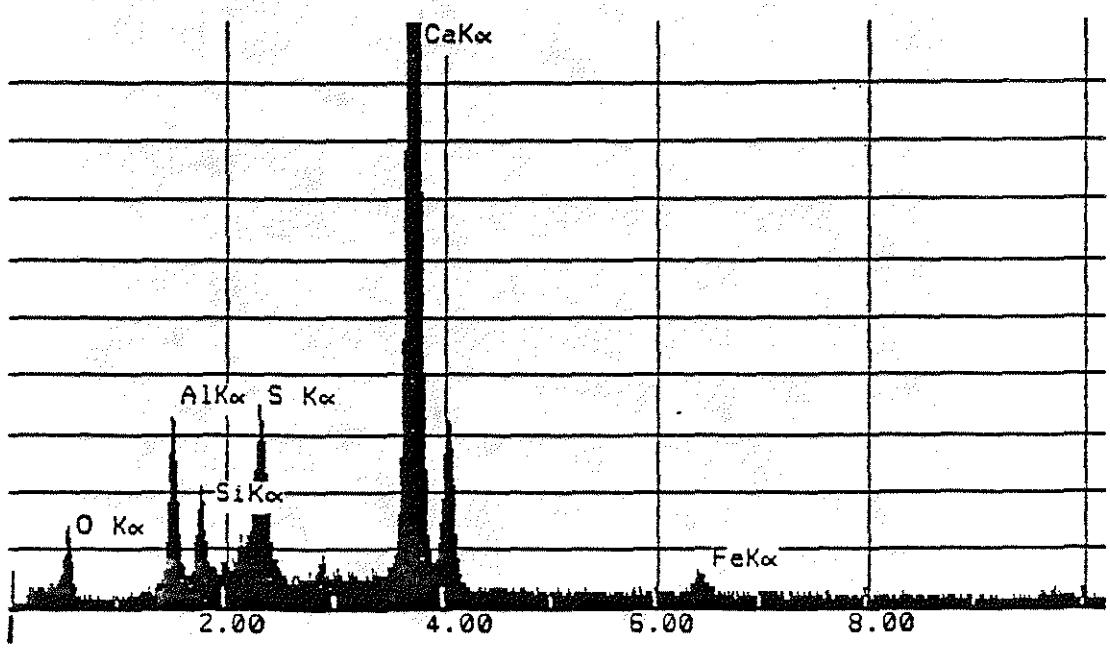

(b)

Fig. 3 X-ray spectra, with SEM in point mode: (a) spectrum for point A, (b) spectrum for point B in Fig. 2.

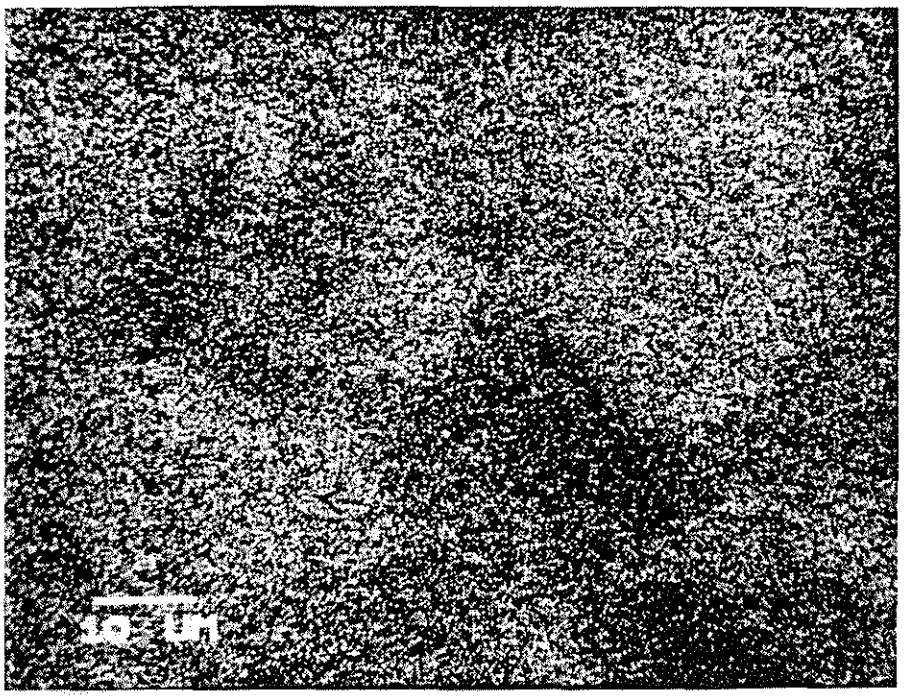

(a)

(b)

Fig. 4 (a) Si Kα x-ray dot map and (b) Fe Kα x-ray dot map of Fig. 2.

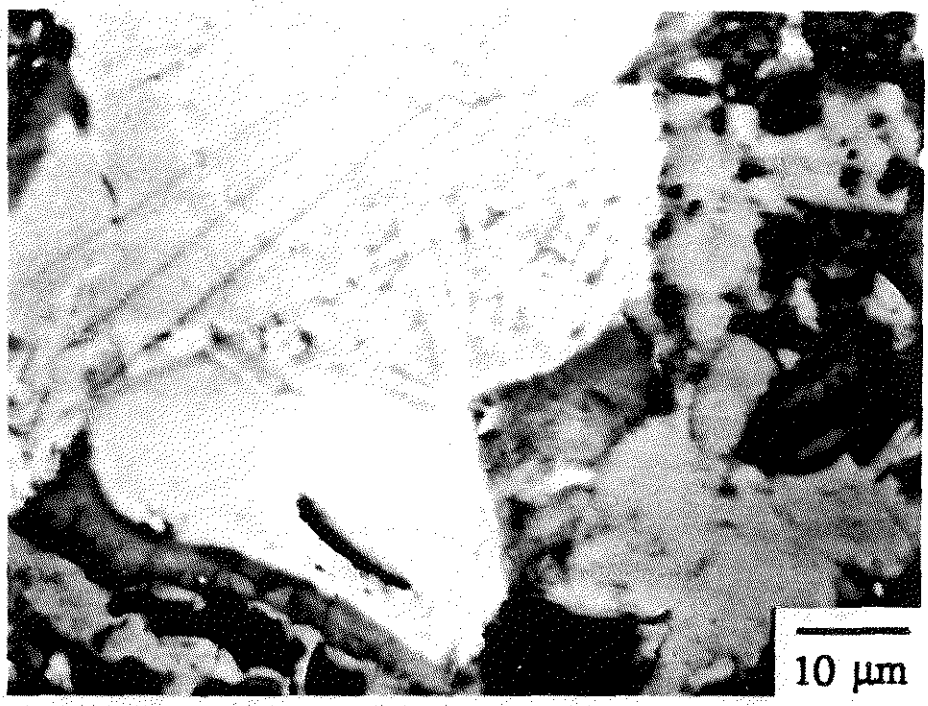

Fig. 5 BSE image of C_4AF phase in unhydrated cement particles.

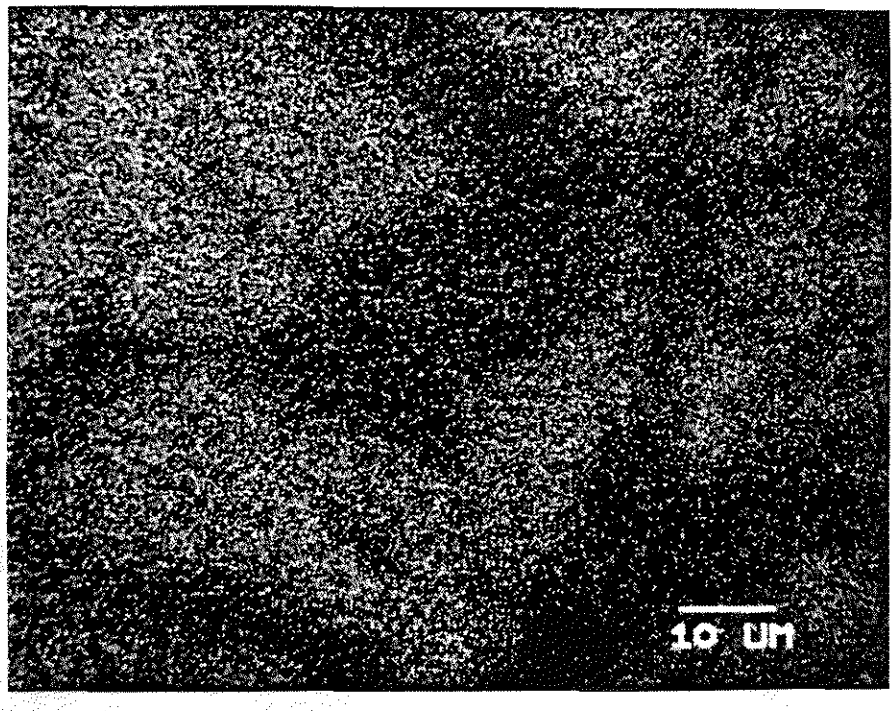

(a)

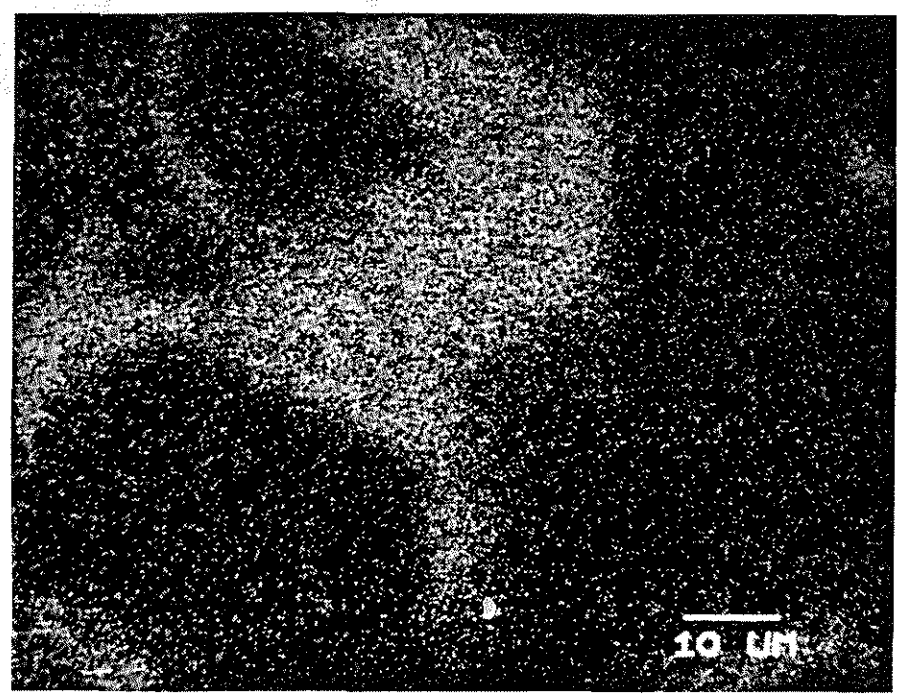

(b)

Fig. 6 (a) Si Kα x-ray dot map and (b) Fe Kα x-ray dot map of region in Fig. 5.

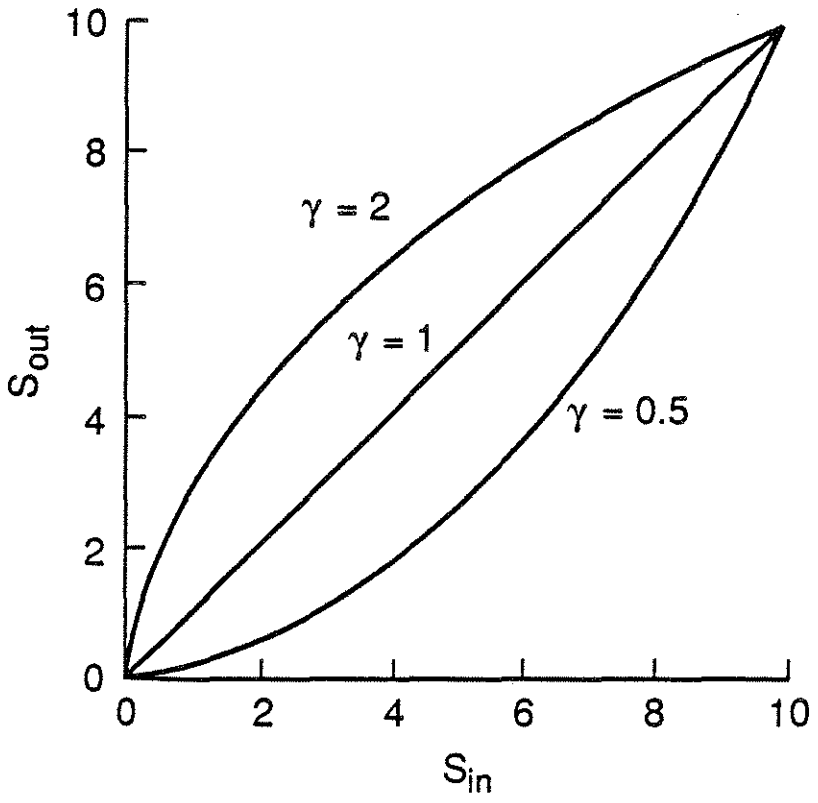

Fig. 7 Signal response curve for nonlinear amplification (γ processing).

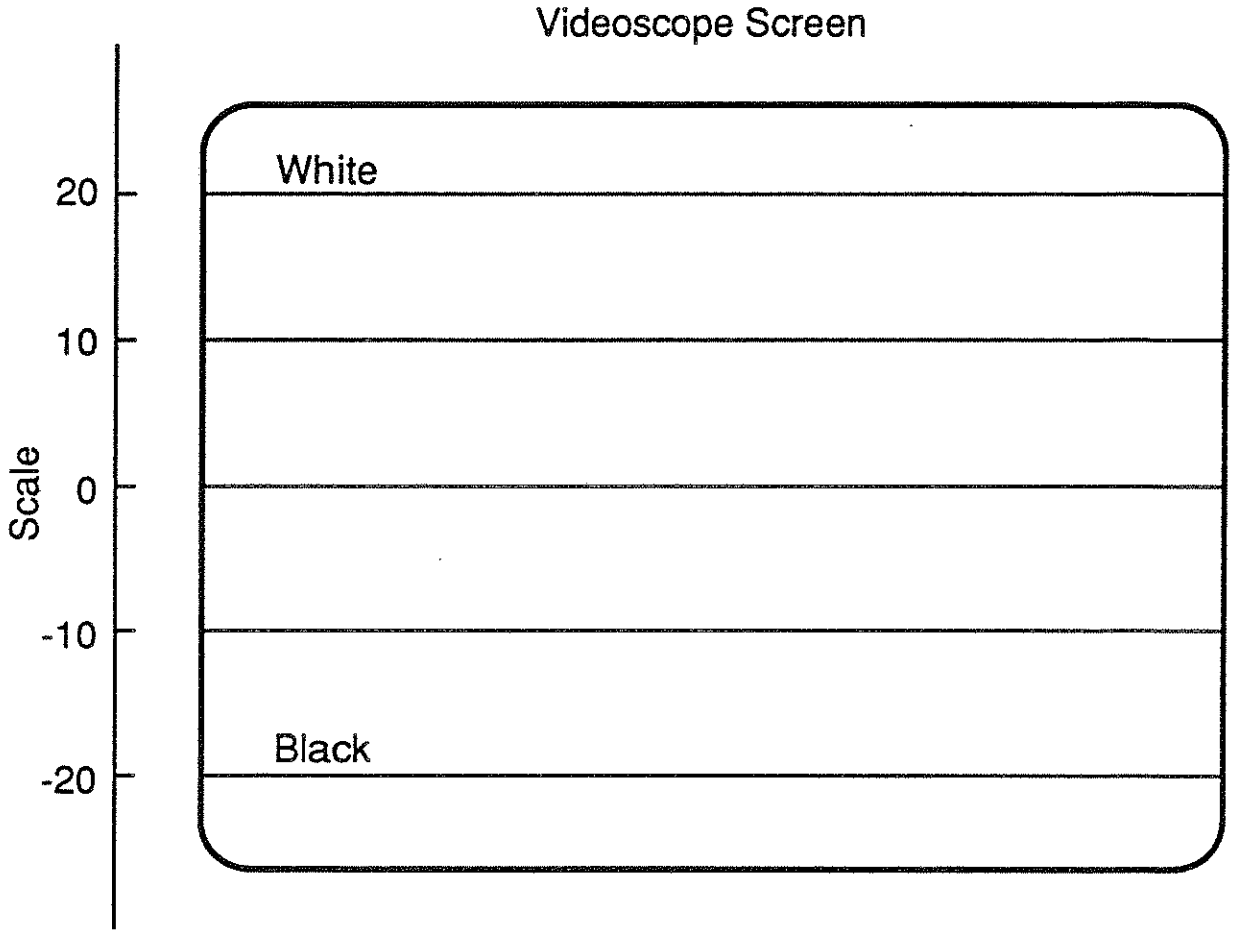

Fig. 8 An artificial scale setup on the videoscope of the SEM.

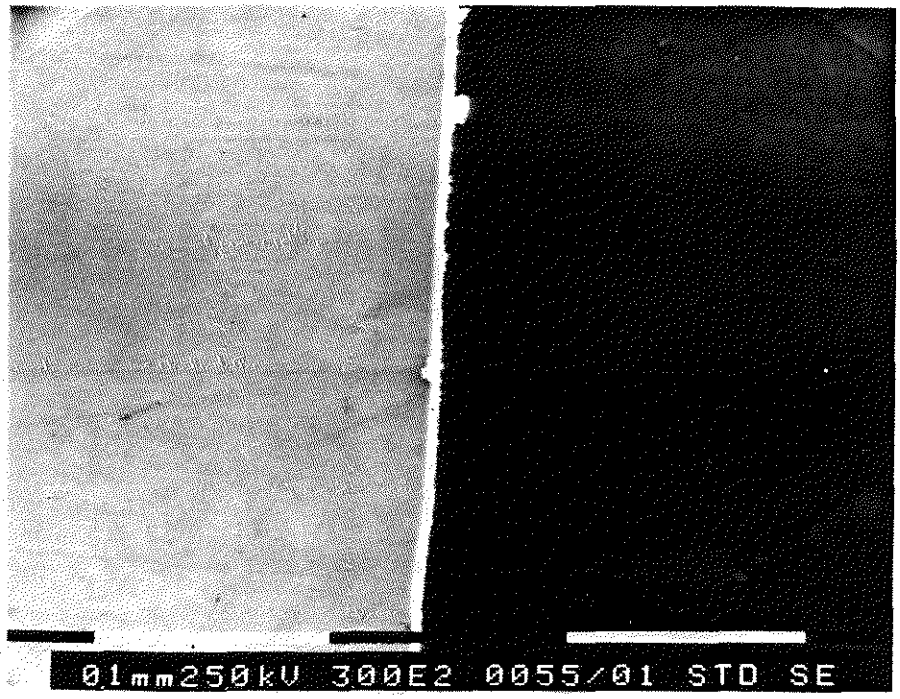

Fig. 9 SE image of the Si-Mg standard at a magnification of 300x.

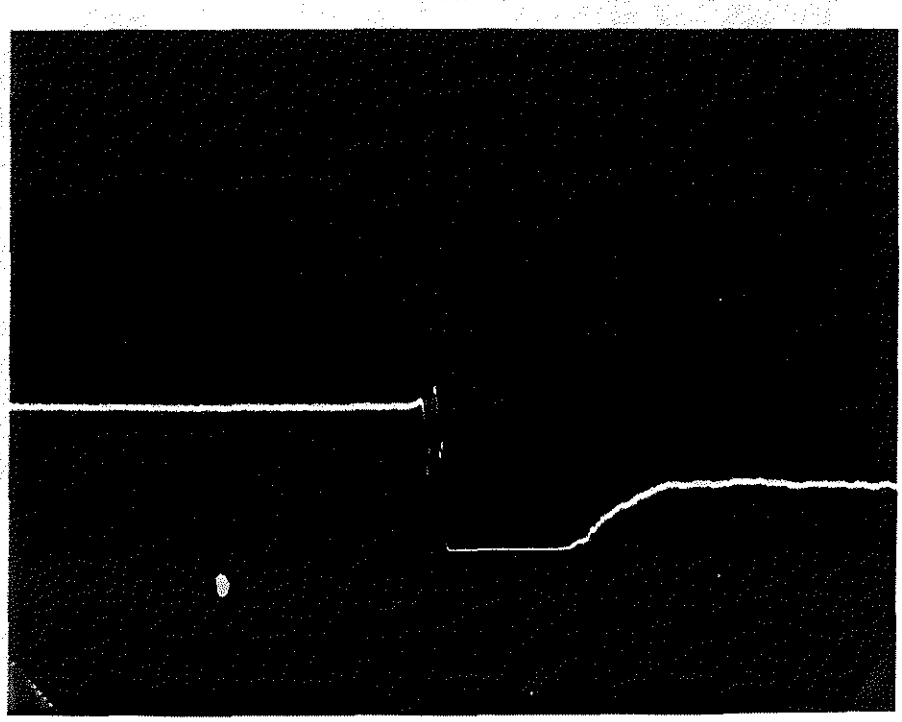

Fig. 10 The step function obtained by imaging at 300x. Line scan mode.

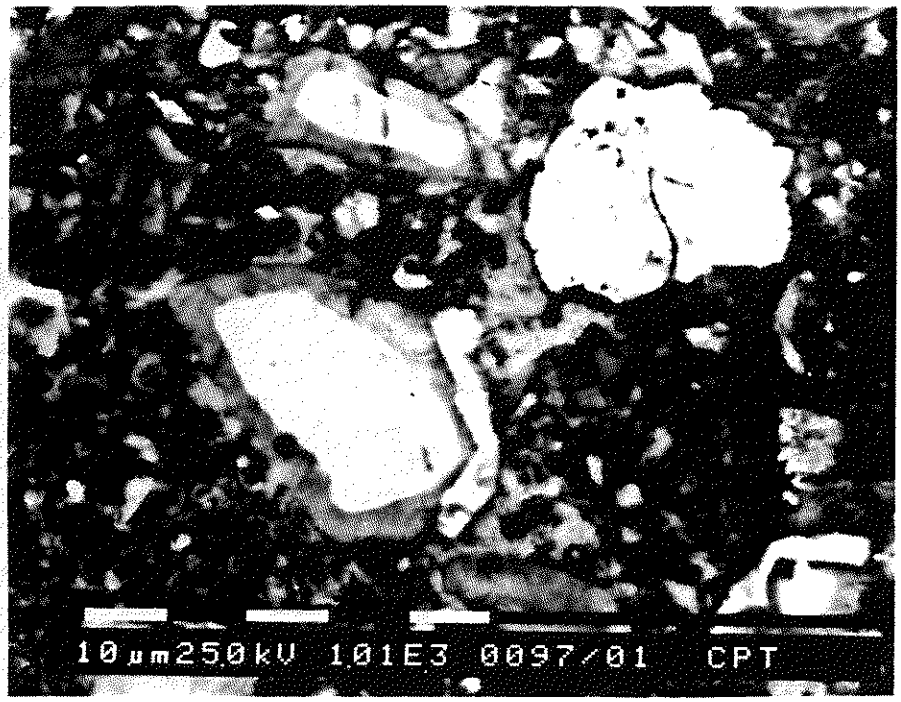

(a)

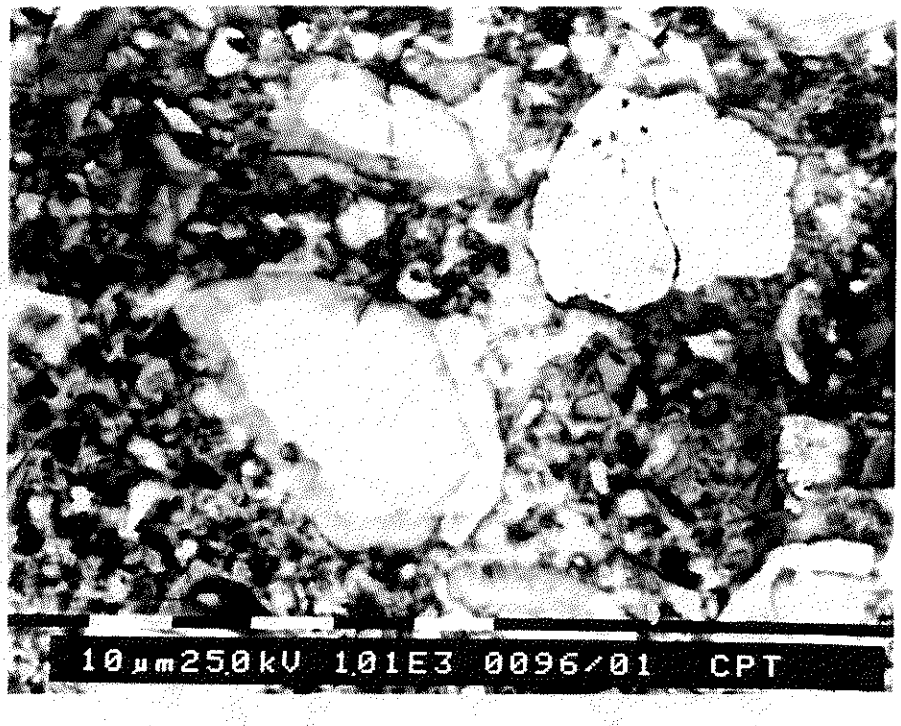

(b)

Fig. 11 Comparison of BSE images (a) without nonlinear amplification, and (b) with nonlinear amplification.

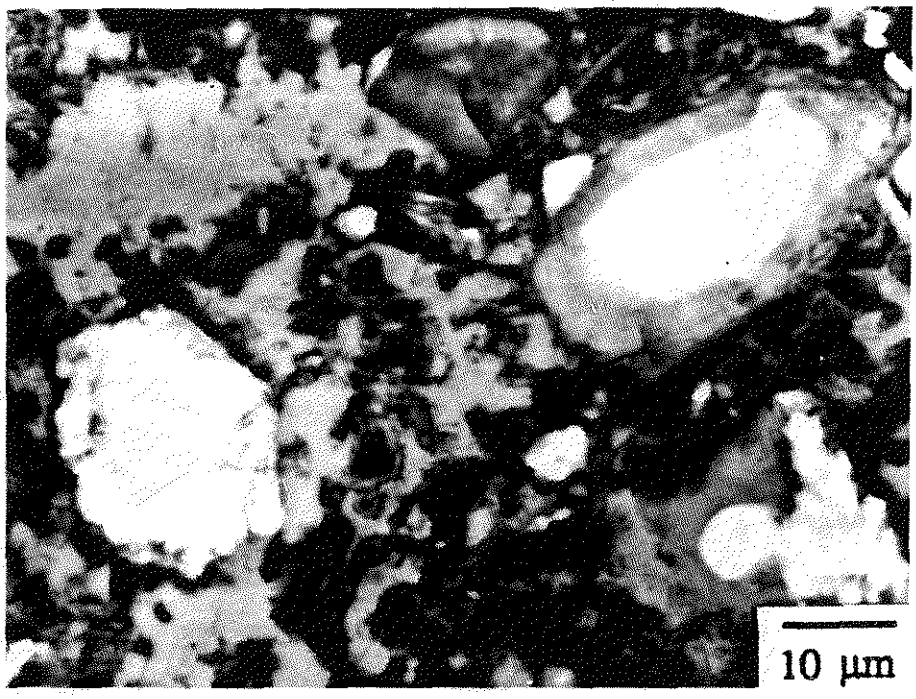

(a)

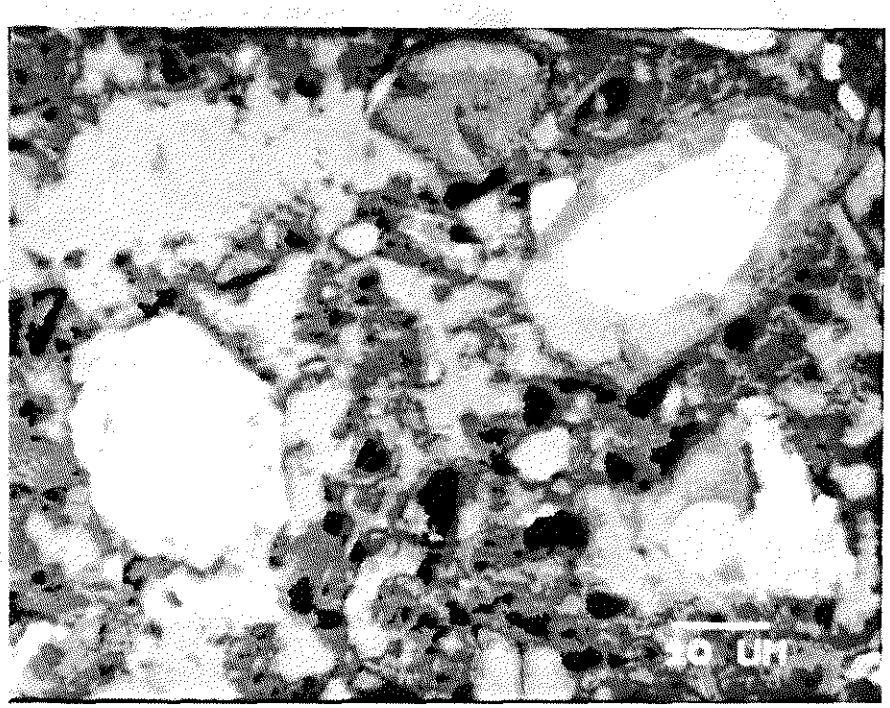

(b)

Fig. 12 (a) A BSE image and (b) its thresheld pseudo-color image.

(a)

(b)

Fig. 13 Comparison of BSE images obtained with (a) Si/Mg = =3/-15, and (b) Si/Mg = -8/-18.

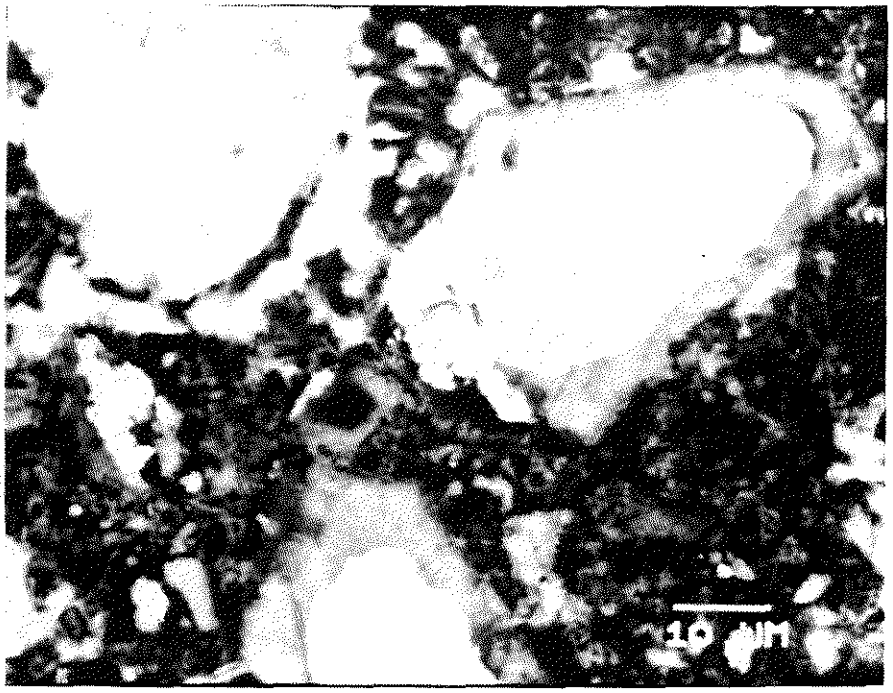

(a)

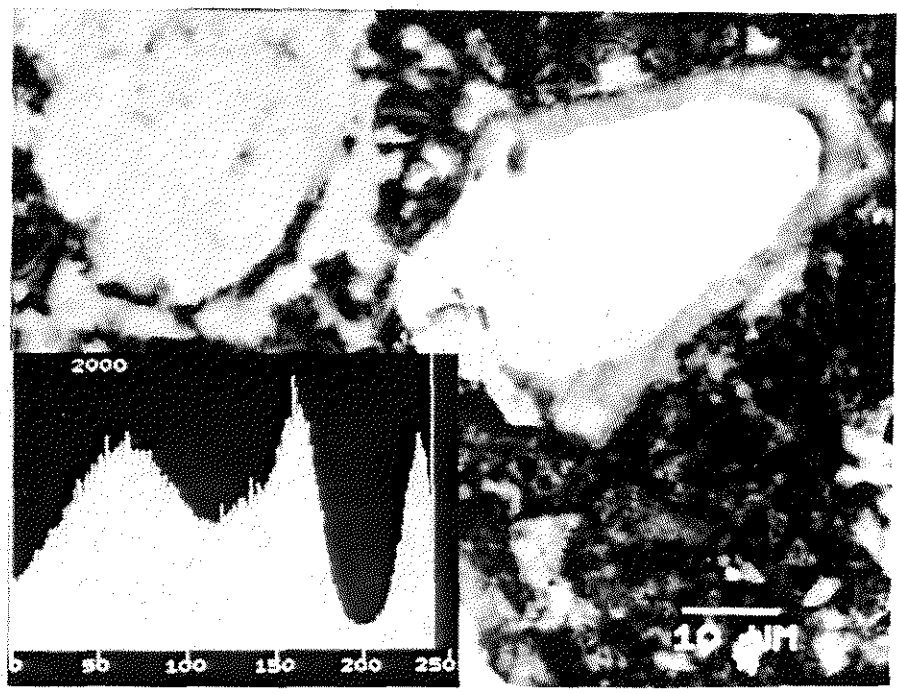

(b)

Fig. 14 (a) BSE image and (b) its gray level histogram display at the maximum contrast (gain = 10) on the IAS.

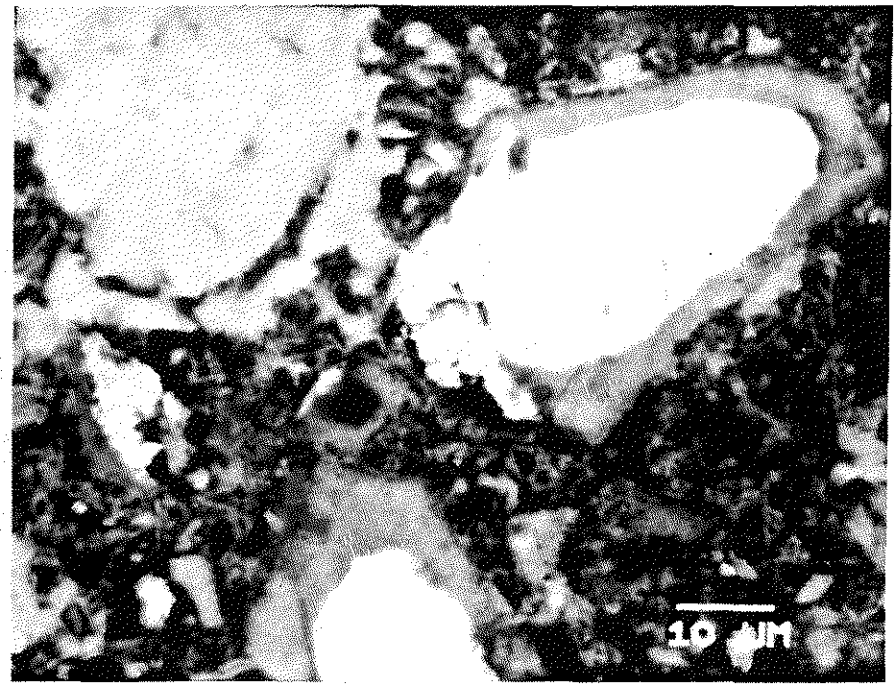

(a)

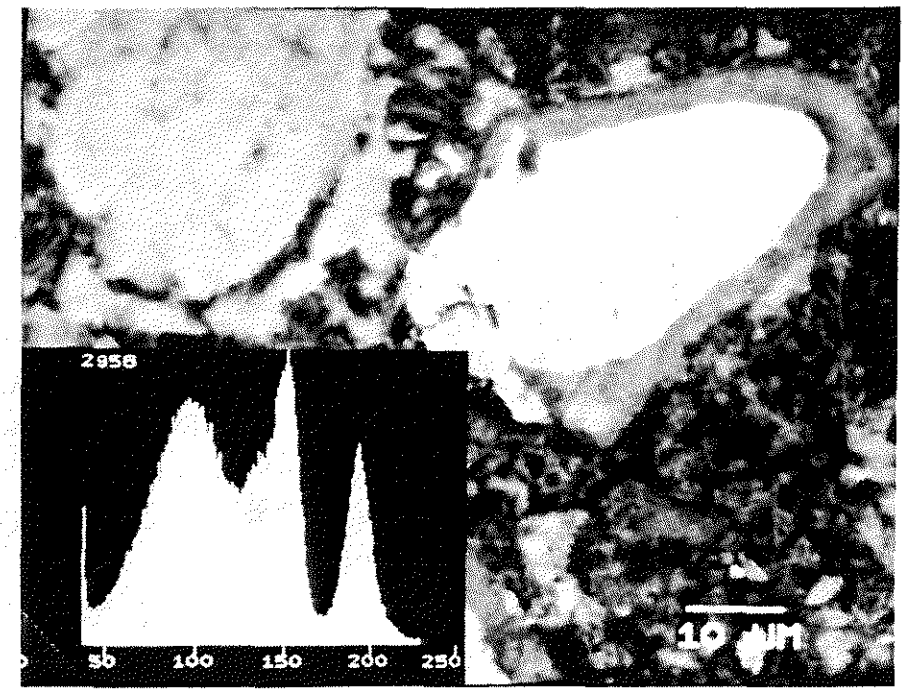

(b)

Fig. 15 (a) The BSE image in Fig. 14 with 75 % of maximum contrast on the IAS, and (b) the gray level histogram display.

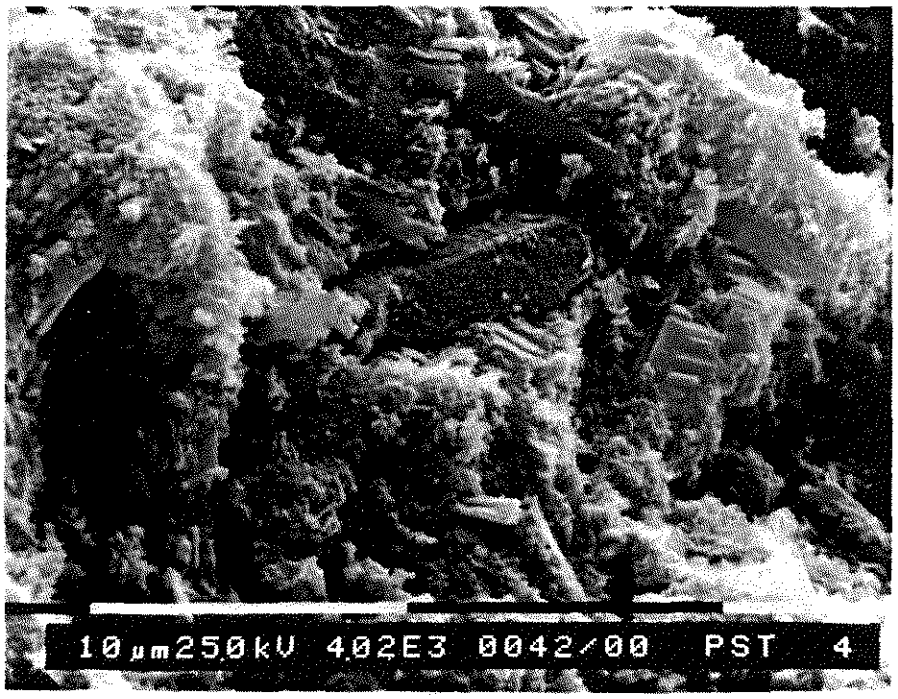

(a)

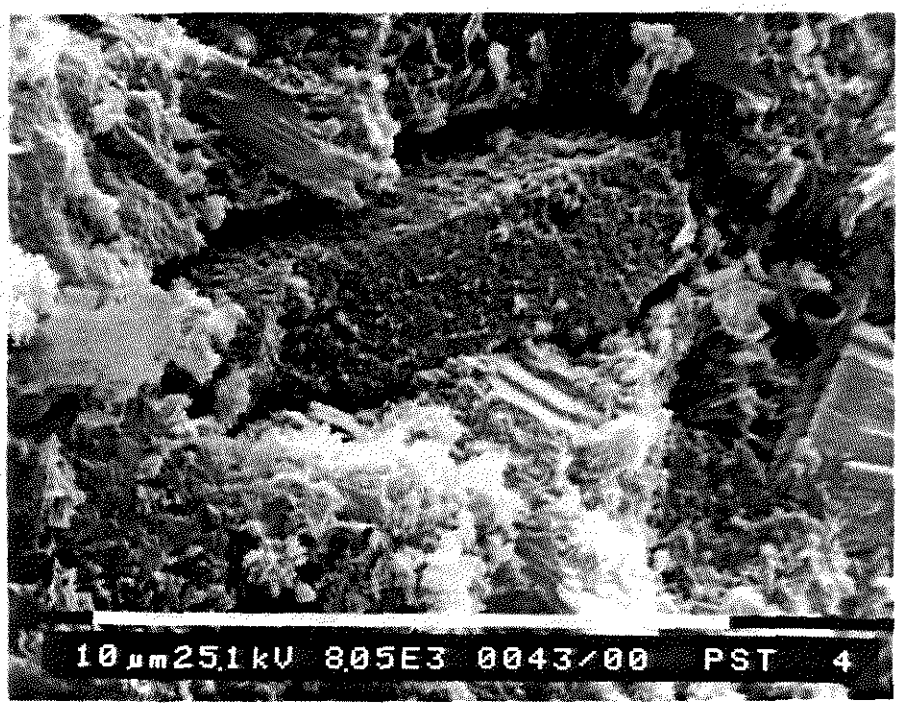

(b)

Fig. 16 SE images of a fractured cement surface at a (a) magnification of 4020x, and (b) a magnification of 8050x.

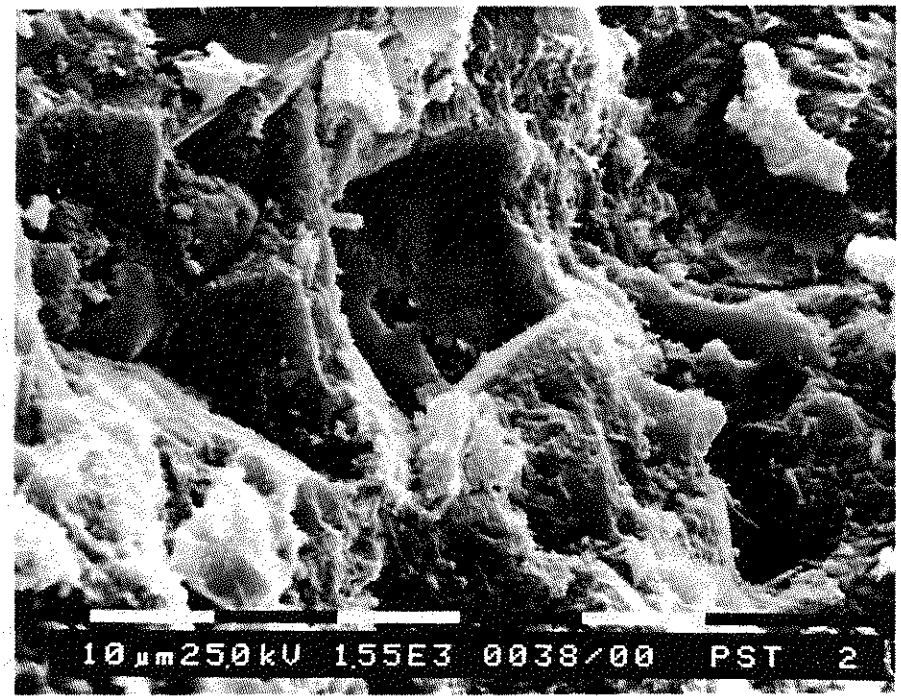

(a)

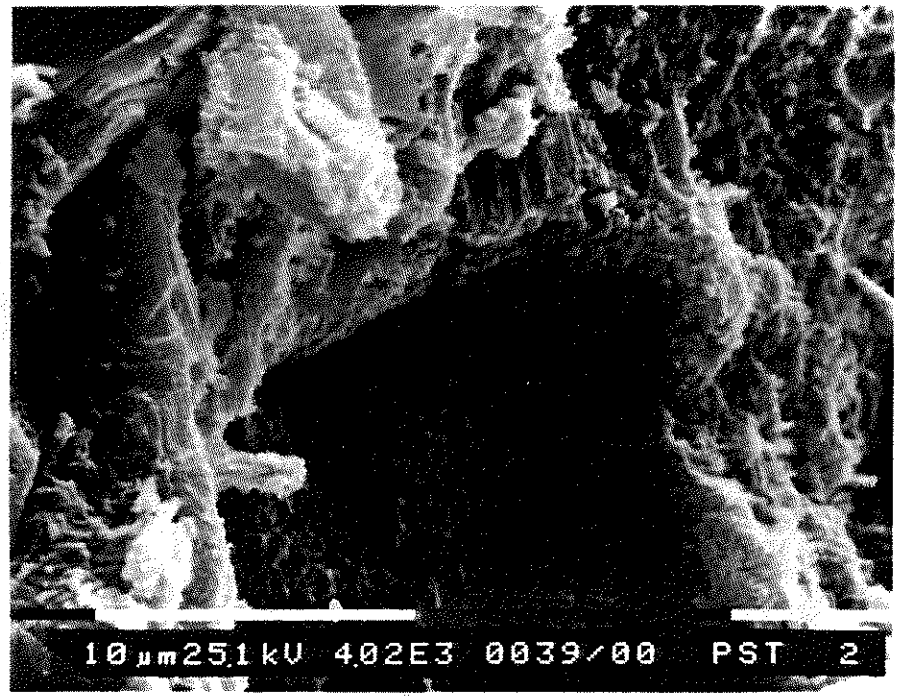

(b)

Fig. 17 SE images of a fractured cement surface at a (a) magnification of 1550x, and a (b) magnification of 4020x.

APPENDIX A

A	Atomic weight
BSD	Backscattered electron detector
BSE imaging	Backscattered electron imaging
C	Contrast
C_i	Weight fraction for element i in a conpound
E_0	Accelerating voltage
EDS	Energy dispersive spectrometer
FWD	Free working distance
IAS	Image analysis system
R_{KO}	Kanaya-Okayama electron range
R_x	X-ray generation range
SE imaging	Secondary electron imaging
SEM	Scanning electron microscope
WDS	Wavelength dispersive spectrometer
Z	Atomic number for pure material
Z	Mean atomic number for compounds
i_B	Beam current
n	Number of frames required in image analysis
n_b	Number of beam electrons
n_{bs}	Number of backscattered electrons
t_f	Frame time
γ	Nonlinear signal processing

ε	Detector efficiency
ε	Acceptable error or half of the maximum acceptable confidence interval
η_1, η_2	Backscattering coefficient for materials 1 and 2
η	Backscattering coefficient for pure materials
η_{mix}	Backscattering coefficient for compounds
ρ	Material density
σ	Standard deviation